



# Study on Shear Mechanical Characteristics of Rock Joints Under Different Anchorage Lengths

Sunhao Zhang<sup>1,2</sup> · Yujing Jiang<sup>1,2,3</sup> · Hengjie Luan<sup>1,3</sup> · Bo Li<sup>4</sup> · Jianrong Liu<sup>3</sup> · Changsheng Wang<sup>1</sup>

Received: 7 September 2023 / Accepted: 9 July 2024

© The Author(s), under exclusive licence to Springer-Verlag GmbH Austria, part of Springer Nature 2024

## Abstract

Understanding the shear characteristics and acoustic emission features of bolted joints is crucial for the optimization of support systems and disaster early warning. In this paper, a series of shear tests on rock joints using both full-length anchorage and partial anchorage methods were conducted. The evolving patterns of shear mechanical characteristics and acoustic emission features of bolted rock joints were obtained, elucidating the influence of anchorage methods and revealing the shear failure mechanisms of joints under different anchorage lengths. The results indicate that the “pin effect” of the bolt can be rapidly mobilized in the full-length anchorage compared to the partial anchorage method. The full-length anchorage exhibits higher peak shear stress and fracture shear stress, with maximum differences of 0.38 MPa and 0.08 MPa, respectively, when contrasted with the partial anchorage method. The deformation range of bolts in the partial anchorage method approximately doubles that observed in the full-length anchorage. Acoustic emission feature parameters exhibit a good correspondence with shear stress curves, and their evolution suggests that the most significant damage to bolted joints occurs at the shear stress peak, with the highest energy release observed when bolts fail. Under both partial anchorage and full-length anchorage, with an increase in normal stress or JRC, the  $b$  of bolted joint acoustic emissions gradually decreases. Compared to the partial anchorage method, the full-length anchorage demonstrates a higher maximum Hit rate, along with lower maximum energy release, implying more intense interaction between bolts and surrounding rock in the full-length anchorage, resulting in greater damage under the same conditions, whereas the deformation range of bolts is smaller, and the energy released upon failure is lower in the full-length anchorage.

## Highlights

- A series of shear tests on rock joints using full-length and partial anchorage methods.
- Investigated the effects of anchorage lengths, normal stress, and joint surface roughness on shear behavior and acoustic emissions.
- The effects of the anchorage lengths on the fracture behavior of bolted joints was revealed.

**Keywords** Rock joint · Anchorage length · Joint surface roughness · Shear strength · Acoustic emission

✉ Hengjie Luan  
luanjie0330@126.com

<sup>1</sup> State Key Laboratory of Mining Disaster Prevention and Control Co-Founded By Shandong Province and the Ministry of Science and Technology, Shandong University of Science and Technology, Qingdao 266590, China

<sup>2</sup> Graduate School of Engineering, Nagasaki University, Nagasaki 852-8521, Japan

<sup>3</sup> Academician (Expert) Workstation of Inner Mongolia Shanghai Mining Co., Ltd, Ordos 016299, China

<sup>4</sup> College of Civil Engineering, Tongji University, Shanghai 200092, China

## 1 Introduction

The widespread occurrence of rock joints can significantly reduce the strength and stability of rock masses, leading to instability in rock engineering projects (Jiang et al. 2004; Wang et al. 2024). Anchoring support can limit interlayer displacement or sliding of joint blocks to enhance rock mass stability. It has been widely applied in various rock engineering reinforcement fields such as mining, tunnels, water conservancy, and slopes (Liu et al. 2017). However, when rock joints experience shear displacement, bolts are prone to failure near the joint due to the combined action of axial and shear forces (Liu et al. 2018a). In recent years, with the continuous expansion of the engineering scale and the increasing complexity of the existing environment, the issue of engineering rock mass instability caused by bolt failure has become more prominent (Li et al. 2022a; Xie et al. 2019). Therefore, understanding the shear characteristics of bolted joints is crucial for controlling the stability of rock engineering projects.

Currently, scholars have conducted extensive research on the shear characteristics of bolted joints using methods, such as laboratory testing, theoretical analysis, and numerical simulation. Laboratory testing is the most commonly used method for studying the shear characteristics of bolted joints, and factors currently considered mainly include boundary condition (Chen et al. 2018a), rock strength (Jiang et al. 2023a), joint surface roughness (Wu et al. 2018a), bolt type (Chen et al. 2015; Grasselli 2005), bolt surface morphology (Wang et al. 2022; Zhang et al. 2020a, b), number of bolts (Srivastava et al. 2015; Chen et al. 2020), bolt inclination angle (Cui et al. 2020), and bolt pre-tensioning (Liu et al. 2012). Through the aforementioned research, researchers have gained preliminary insights into the shear mechanical characteristics and failure behavior of bolted joints. They have revealed the influence patterns of individual factors on the shear characteristics of bolted joints. Numerical simulations can expand and enhance the results of laboratory testing by providing information about internal stress, strain, and damage evolution within rocks and bolts that are difficult to measure in the laboratory. Li et al. (2019), Bahrani et al. (2017), Lin et al. (2014), Fan et al. (2023), and He et al. (2019) have conducted numerical simulations of shear behavior on bolted joints using finite element analysis and discrete element methods. These studies have further clarified the shear characteristics of bolted joints and deepened the understanding of the mechanisms underlying their shear resistance. Theoretical analysis is another effective method for studying the shear resistance of bolted joint, which focuses on shear strength calculation. Ge et al. (1988) proposed that “the shear strength of a bolted joints is composed of the joint surface’s inherent shear strength

and the shear strength respectively contributed by equivalent forces provided by bolts acting along the normal and shear directions of the joint surface”. This perspective has been widely accepted, based on which Liu et al. (2018a, b), Chen et al. (2018b), and Ma et al. (2019) have conducted research on key issues such as the geometric model of bolts, the distribution characteristics of constrained forces on bolts, yielding patterns and criteria of bolt; then, they subsequently developed theoretical models for the shear strength of bolted joints, which were validated through laboratory testing. While these studies are significant in revealing the shear mechanical characteristics of bolted joints, they lack an in-depth understanding of the internal deformation, failure, and damage evolution of rocks and bolts.

Acoustic emission (AE) technology enables dynamic and non-destructive monitoring of micro-damage signals within rocks (Chen et al. 2023). Analyzing the evolution of AE parameters (hit and energy) is beneficial for better understanding the micro-damage evolution of rocks during shear processes. As a result, AE technology has found widespread application in both laboratory experiments and field microseismic monitoring (Meng et al. 2016, 2019; Hu et al. 2023). While AE technology has been extensively used in uniaxial (Wang et al. 2021, 2023), triaxial (Yu et al. 2022; Jia et al. 2020), and rock joint shear tests (Zhang et al. 2020a, b; Liu et al. 2022), its application in monitoring the shear behavior of bolted joints is relatively limited. Hu et al. (2023) carried out rock bridge shear tests and large-scale physical tests to investigate the signals released during rock bridge failure, providing a theoretical basis for early warning of tunnel disasters. Wang et al. (2018) have used AE technology to analyze the impact of factors including normal stress, joint surface roughness, and bolt type on AE characteristics of bolted joints. Similarly, Li et al. (2022b) employed AE technology to monitor shear behavior in bolted joint shear tests, investigating the influence of factors such as normal stress, bolt inclination angle, and joint surface roughness on the evolution of microcracks during shear. To reveal the shear failure characteristics of deeply bolted rock masses, Li et al. (2023) conducted high-stress bolted joint shear tests, combined with AE technology to explore stress drop events and the evolution of dynamic failure strength during shear processes. The mentioned studies demonstrate that acoustic emission technology can effectively monitor the evolution of microcrack count and energy in bolted joints during shear processes. However, most of these studies have been conducted with full-length anchorage. Partial anchorage are also widely used in engineering projects such as coal mine roadway (Yan et al. 2019; Li et al. 2016; Yang et al. 2017a, b). In China, 13,000 km of roadway are excavated each year, equivalent to the diameter of the earth (He. 2017; He et al. 2021). Most of this is done using the

partial anchorage. In partial anchorage, its free segment (unanchored part) is in the fracture zone of the surrounding rock, which is often affected by the shear slip of the fractures in the surrounding rock, causing shear failure (Wu et al. 2019; Li et al. 2017). When grout is not present at joint locations, the stress and deformation characteristics of bolts can be significantly different, suggesting that revealing the impact of different anchorage lengths on the shear characteristics and damage evolution of bolted joints holds significant importance. Chen et al. (2020) carried out a laboratory and theoretical analysis of the anchoring effectiveness of partial anchorage and full-length anchorage in layered jointed rock. Teng et al. (2017) carried out double shear tests under different anchorage lengths and analyzed the shear behavior of rock joints and the force deformation behavior of bolts in three cases, namely no bolt, end bolt and full bolt. Feng et al. (2024) carried out double shear tests under partial anchorage and the evolution law of internal forces and failure mechanism of the free section of the partial anchorage cable under tension–shear action were revealed by theoretical analysis. The above studies have carried out a preliminary investigation of the shear behavior of bolted joints under different conditions of anchorage lengths and have produced some useful results. These studies were carried out under uniaxial or double shear conditions and it is difficult to quantitatively control the normal stress on the joint. Bolted joint direct shear test research under different anchorage lengths is still unreported.

Given the understanding outlined above, it is essential to carry out shear tests on bolted joints with different anchorage lengths. However, it is difficult to carry out in situ tests. Therefore, a constant similarity ratio was applied to downscale the test parameters, and a series of shear tests on rock joints under both full-length and partial anchorage were conducted in the laboratory, revealing the evolution patterns of bolted joint shear strength, joint surface damage, bolt deformation and failure, and acoustic emission characteristics. Moreover, the influence of anchorage lengths, normal stress, and joint surface roughness on these aspects was elucidated, and the shear damage and failure mechanisms of rock joints under different anchorage lengths were analyzed. The research results enrich the understanding of shear characteristics and bolt reinforcement mechanisms of bolted joints. At the same time, it provides important data for determining the precursor information of bolted joint breakage. This holds practical significance in enhancing rock engineering safety and protection, as well as optimizing support systems and disaster early warning.

## 2 Test Method

### 2.1 Sample Preparation

High-strength gypsum material with a 1:0.2:0.005 mass ratio of gypsum, water, and retarder was selected to prepare rock-like joint specimens in this study. The material has a uniaxial compressive strength of 47.4 MPa and an elastic modulus of 28.7 GPa, and has achieved good application results in previous rock mechanics tests (Jiang et al. 2004). Using rock-like materials aims to make a large number of joint specimens with the same surface morphology, thereby overcoming the variation in shear strength caused by differences in joint surface characteristics.

As is well known, the accuracy of test results depends on the similarity of the supporting materials used in tests. The diameter, length, fracture force, and modulus of elasticity of the model bolts should meet the similarity criterion. However, when choosing the model bolt, it is difficult to fully meet similarity criterion. The primary function of bolts in support engineering is to provide radial restraint and to reinforce loose rock masses. Therefore, the fracture force of bolts is chosen as the main criterion for the selection of model bolts (Jing et al. 2014). The formula is as follows (Yu et al. 2021):

$$C_F = \frac{F_1}{F_2} = \frac{\sigma_1 A_1}{\sigma_2 A_2} = C_L^2 C_\sigma \quad (1)$$

$$C_\sigma = C_\gamma C_L \quad (2)$$

$$C_F = C_L^3 C_\gamma, \quad (3)$$

where  $C_F$  is the similarity ratio of fracture force;  $F_1$  is the characteristic parameter of the prototype fracture force;  $F_2$  is the characteristic parameter of the model fracture force;  $\sigma_1$  is the characteristic parameter of the prototype stress;  $\sigma_2$  is the characteristic parameter of the model stress;  $A_1$  is the characteristic parameter of the prototype cross-sectional area;  $A_2$  is the characteristic parameter of the model cross-sectional area;  $C_L$  is the geometric similarity ratio,  $C_L = L_1/L_2$ ,  $L_1$  is the characteristic parameter of the prototype geometry,  $L_2$  is the characteristic parameter of the model geometry;  $C_\gamma$  is the density similarity ratio,  $C_\gamma = \gamma_1/\gamma_2$ ,  $\gamma_1$  is the characteristic parameter of the prototype density, and  $\gamma_2$  is the characteristic parameter of the model density.

The density of the rock-like materials in this paper is comparable to the general rock densities (Jiang et al. 2004) and  $C_\gamma$  can be considered as 1. Typical bolt parameters are given in Table 1. Based on the dimensions of the bolted joint specimens, it can be calculated that  $C_L = 2.3\text{--}4.2$ , where in this study 2.4 is used. According to formula 1,  $C_F = 13.8$ ,

**Table 1** Mechanical behavior of steel bolt used in coal mine engineering practice (Jing et al. 2014)

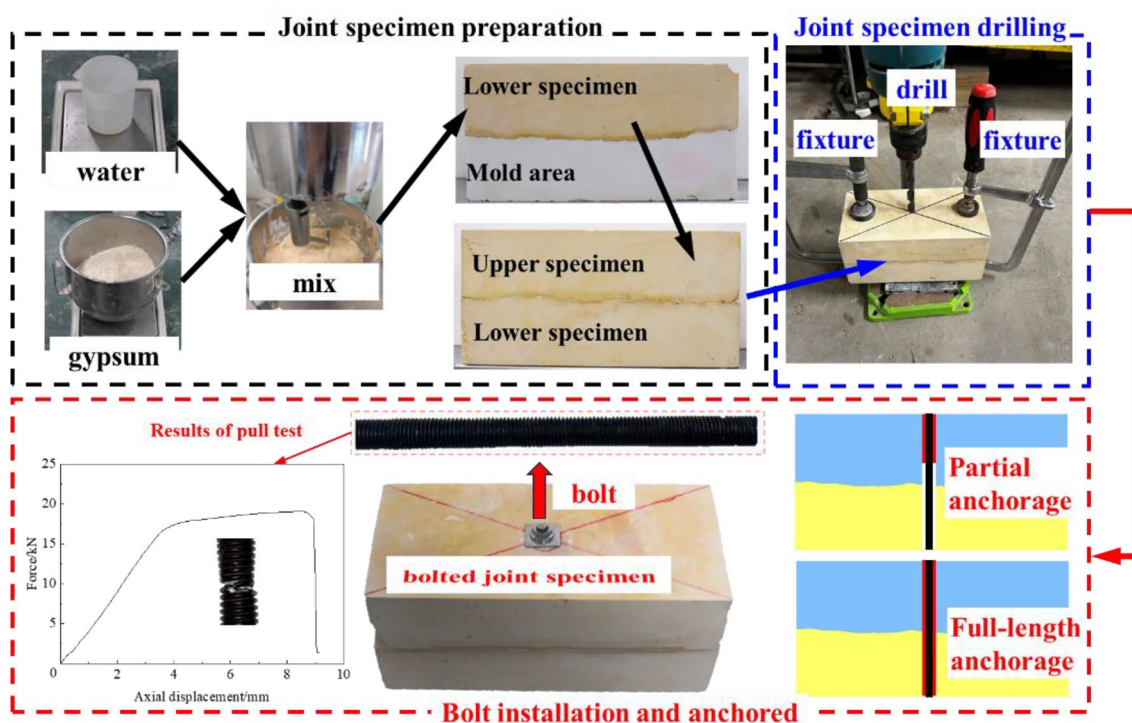
Diameter (mm)	Yielding strength (MPa)	Limiting strength (MPa)	Elastic modulus (GPa)	Yielding load (kN)	Fracture load (kN)	Extensibility (%)
16–25	340	520	210	68.4–129.2	106.6–270.4	≥ 16

which means that the fracture forces of the bolts in the tests should be between 7.7 and 19.6 kN. Therefore, in this study, surveys and tests were carried out on commercially produced bolt. In the end, a 6 mm-diameter bolt made of 8.8 grade carbon steel with a fracture force of 19.1 kN was selected using the principles of similarity. The results of the pull-out tests are shown in Fig. 1. In the test, the length of the bolt is 110 mm and each end of the bolt extends 5 mm beyond the joint specimen to install nuts and washers.

The properties of the grout significantly impact the shear stress of the bolted joint. The influence of grout properties on the strength of bolted joints is evident in two primary aspects: first, increased grout strength enhances the axial force near the joint surface of the bolt; second, it leads to a narrower range of bolt deformation, thus affecting its failure mode. In reference to previous studies (Wu et al. 2018a, b; Zhang et al. 2022), the grout selected for the tests comprised high-strength gypsum with a gypsum-to-water mass ratio of 1:0.32.

The fabrication process of the bolted joint specimens is shown in Fig. 1; After the joint specimens were poured and cured for 2 weeks, holes were drilled using an electric drill. After cleaning the hole walls, bolts were installed and anchored using the grout. The diameter of the borehole in the test was 10 mm. The grout lengths of the full-length anchorage and partial anchorage were set to 100 mm and 30 mm, respectively, with reference to the relevant literature (Kang et al. 2014; Zhang et al. 2022). During grouting process, the joint specimens were clamped with a fixture to ensure the tight closure of joints and then prevent the grout bonding to the joint surfaces.

In this study, three joint surfaces with different roughness levels were selected for specimen preparation, which were labeled as J1, J2, and J3. Figure 2 displays the joint surface morphology obtained through 3D scanning. Using the slope root mean square method, values of JRC were calculated for the three joint surfaces based on 3D scan data. Initially, 50 curves along the shear direction were selected on each joint

**Fig. 1** Production process of bolted rock joints

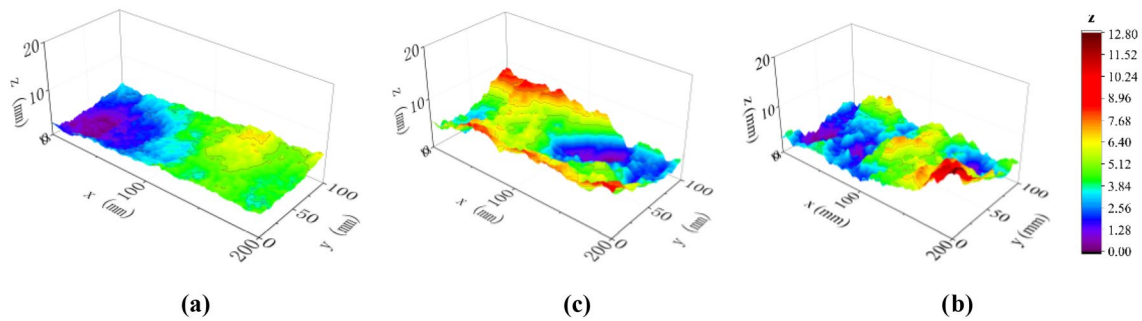


**Fig. 2** Surface topographies of rock joints with different JRCs: **a** JRC=3.68; **b** JRC=6.18; **c** JRC=9.86

surface at 2 mm intervals, and the JRC of each curve was calculated using the following formula (Tse et al. 1979):

$$Z_2 = \sqrt{\frac{1}{(n-1)(\Delta x)^2} \sum_{i=1}^{n-1} (Z_{i+1} - Z_i)^2} \quad (4)$$

$$\text{JRC} = 32.2 + 32.47 \log Z_2, \quad (5)$$

where  $Z_2$  represents slope root mean square;  $\Delta x$  represents the interval between data;  $n$  is the number of data points on each curve;  $Z_i$  represents the coordinate  $z$  for each curve.

Subsequently, the average value of JRC from the 50 curves was taken as the JRC value for each joint surface. Finally, the calculated JRC values for J1, J2, and J3 were 3.68 (corresponding to 2–4 in the Barton curve (Barton et al. 1977)), 6.18 (corresponding to 6–8 in the Barton curve), and 9.86 (corresponding to 8–10 in the Barton curve), respectively.

## 2.2 Experiment Apparatus

The experiments were conducted using the MIS-233–1–55–03 constant normal stiffness servo-controlled shear testing system, as depicted in Fig. 3 (Jiang et al. 2004). The normal force and shear force in this testing system were applied using vertical and horizontal jacks, respectively. The system can provide a maximum normal force and shear force of 200 kN, enabling the application of constant normal load (CNL) in the normal direction and constant normal stiffness (CNS) boundary conditions. The upper part of the shear box remained fixed horizontally during the shearing process, while the lower part of the shear box was pushed to induce displacement along the joint. During the experiment, LVDT displacement transducers were used to monitor the displacement of the joint in both the normal and horizontal directions, whose accuracy and measurement range were 0.001 mm and 0–20 mm, respectively.

During the shear process, the acoustic emission signals were monitored using an eight-channel PAC-AEwin system.

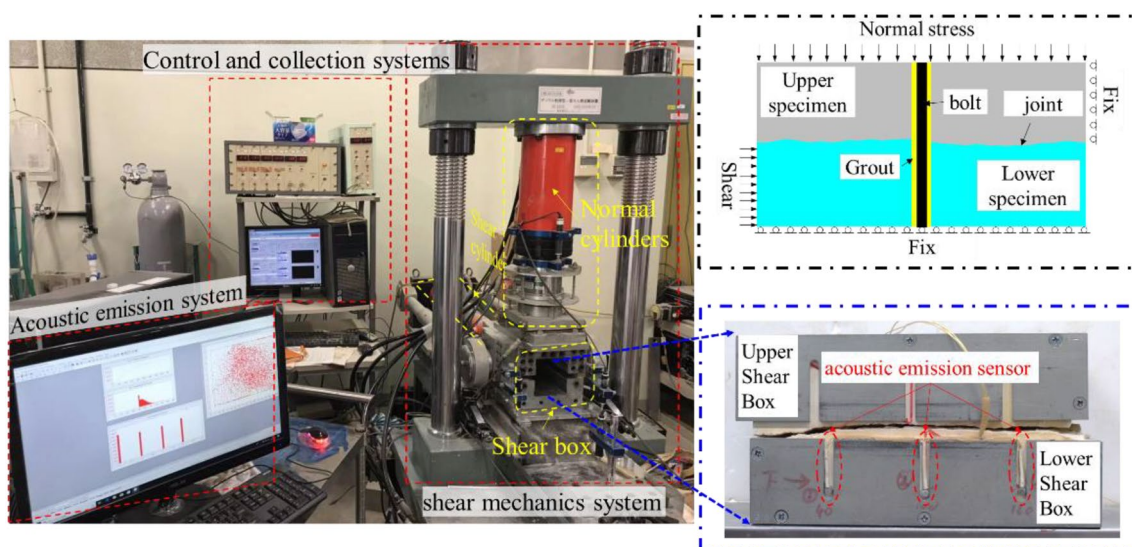


**Fig. 3** The shear experiment system

The acoustic emission sampling rate was set at 5 MSPS (5 million samples per second), with the amplification factor of the front-end amplifier and the system threshold both set to 40 dB. 6 PICO sensors were employed to record the acoustic emission signals, with 3 sensors positioned on each side as depicted in the bottom right corner of Fig. 2.

### 2.3 Test Scheme

The experiments were conducted under the CNL boundary condition with normal stresses of 2 MPa, 4 MPa, and 6 MPa applied. During the experiment, the normal stress of the test specimen was first loaded to the specified value at a rate of 0.5 MPa/min. Subsequently, the lower part of the shear box was pushed at a rate of 0.5 mm/min until the shear displacement reached the target value, at which point the loading was stopped. This is because the bolt failure displacement is greater in the partial anchorage than in the full-length anchorage, and the load-bearing capacity of the anchored joint after bolt failure is no longer the focus, so different shear displacements need to be set. The shear displacement target values for full-length anchorage and partial anchorage were 10 mm and 15 mm, respectively. To better understand the influence of anchorage lengths on the shear characteristics of rock joints, shear tests were also conducted on unbolted joints for comparison. The specific experimental plan is listed in Table 2.

## 3 Shear Mechanical Characteristics of Bolted Joints

### 3.1 Shear Stress–Displacement Curve

The typical shear stress–shear displacement curves for joints under unanchored, full-length anchorage and partial anchorage conditions are shown in Fig. 4. It is evident that the evolution trend of shear stress–shear displacement curves varies significantly. Considering that numerous researchers have already provided comprehensive descriptions of shear stress–shear displacement curve characteristics for joint (Jiang et al. 2023b, c), this paper will instead focus on the analysis of shear stress–shear displacement curve characteristics for full-length anchorage and partial anchorage conditions.

The shear process of fully bolted joints can also be divided into three stages. Stage I:  $I_F$  prepeak stage, which extends from the shear initiation point to the shear stress peak; within this stage, the shear stress linearly increases and rapidly reaches its peak  $\tau_{PF}$ . Stage II:  $II_F$  postpeak stage, which involves the interval from the shear stress peak to the first bolt fracture point; during this stage, the shear strength of the bolted joints exhibits a short-lived declining trend,

**Table 2** Test scheme

Normal stress/MPa			Normal stress/MPa		
Specimen	Roughness	Anchor method	Specimen	Roughness	Anchor method
J1-2-F	3.68	Full-length anchorage	J1-2-E	3.68	Partial anchorage
J1-4-F	4		J1-4-E	4	
J1-6-F	6		J1-6-E	6	
J2-2-F	6.18	Full-length anchorage	J2-2-E	6.18	Partial anchorage
J2-4-F	4		J2-4-E	4	
J2-6-F	6		J2-6-E	6	
J3-2-F	9.86	Full-length anchorage	J3-2-E	9.86	Partial anchorage
J3-4-F	4		J3-4-E	4	
J3-6-F	6		J3-6-E	6	

Note: J1, J2, and J3 represent the joint surfaces with different roughness levels, namely J1, J2, and J3. The numbers 2, 4, and 6 correspond to the normal stresses of 2 MPa, 4 MPa, and 6 MPa, respectively. The letters F, E, and U indicate full-length anchorage (F), end anchorage (E), and unanchored (U) methods, respectively

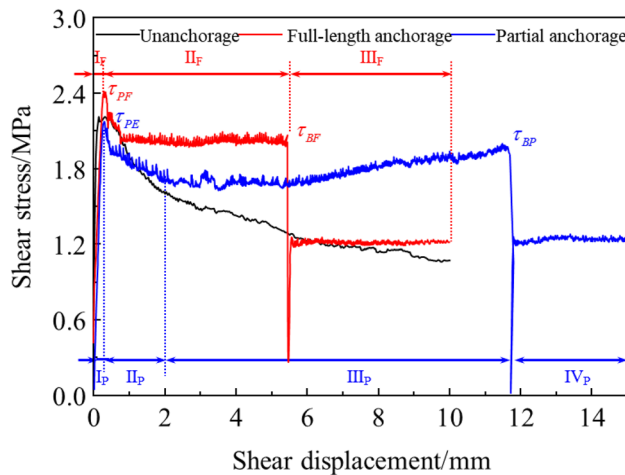


**Fig. 4** Typical shear stress–shear displacement curves for different anchorage lengths

followed by a relatively stable pattern until the bolt fractures. The shear stress at bolt fracture is  $\tau_{BF}$ . Stage III:  $III_F$  post-bolt-fracture, which is characterized by a noticeable step-like drop in the shear stress–shear displacement curve, followed by a generally lower value that roughly continues the trend of the previous stage.

The shear process of partially bolted joints can be divided into four stages. Stage I:  $I_P$  prepeak stage, which is similar to the first stage of the previous two anchorage lengths. The shear stress of the partially bolted joints rapidly increases until the shear stress peak  $\tau_{PP}$ . However, it needs to be noted that the shear stress peak  $\tau_{PP}$  is close to the shear stress peak in the unanchored case  $\tau_{PU}$ , and lower than the shear stress peak in the full-length anchorage case  $\tau_{PF}$ . This is because the bolts near the joint are not engaged, and the bolts do not yet exert their “pin effect” during this stage. Stage II:  $II_P$  displacement softening stage, which extends from the shear stress peak to the point when the bolts make contact with the surrounding rock. During this stage, the shear stress of the bolted joints is still primarily provided by the joint. Therefore, as the joint surface roughness degrades, the shear stress continuously decreases. Stage III:  $III_P$  shear stress increasing stage, which begins when the bolts make contact with the surrounding rock and continues until the bolts fracture. As the bolts come into contact with the surrounding rock, the shear stress of the entire bolted structure is provided by the joint’s shear resistance and the bolts’ shear resistance. The overall shear stress gradually increases with the shear displacement until the bolts fracture. The shear stress at bolt fracture is  $\tau_{BP}$ . Stage IV:  $IV_P$  post-bolt-fracture stage, which spans from the bolt fracture to the end of shear, follows a similar pattern as Stage  $III_P$  in the full-length anchorage case.

### 3.2 Shear Stress Characteristic

Figure 5 shows the shear stress–shear displacement curves for unanchored, full-length anchorage, and partially bolted joint specimens with different JRC values under varying normal stress conditions. It is evident that due to the influence of anchorage lengths, joint surface roughness, and normal stress, the peak shear stress, fracture shear stress, and residual stress exhibit different evolutionary characteristics. Notably, the residual shear stress for partial anchorage and full-length anchorage cases is almost the same as that for the unanchored case. This is because in this stage, after the bolt fracture, they no longer play a role, and the residual shear stress is provided by the joint surface itself. Therefore, the analysis mainly focuses on the differences in peak shear stress and fracture shear stress. To quantitatively analyze the impact of different anchorage lengths on the evolution of shear stress, the peak shear stress and fracture shear stress for each set of shear stress curves were statistically analyzed, as shown in Table 3.

Based on Table 3, a comparison chart of peak shear stress–normal stress and fracture shear stress–normal stress for both partial anchorage and full-length anchorage conditions was generated, as shown in Fig. 6; it can be observed that the peak shear stress and fracture shear stress of the bolted joints under the full-length anchorage condition are larger than those under the partial anchorage condition; the increase in peak shear stress is more significant, which is primarily due to the fact that in the partial anchorage case, the surrounding rock is not in direct contact with the bolts, and the “pin effect” of the bolts is not fully engaged before the peak shear displacement is reached. As the shear progresses, the bolts start making contact with the surrounding rock, and the shear and tensile strength of the bolts are fully utilized. Therefore, when the bolt fractures, the difference in fracture shear stress between partial anchorage and full-length anchorage bolts is not significant. From Fig. 6, it can be found that as the normal stress increases from 2 to 6 MPa, under the full-length anchorage condition, the peak shear stress of J1, J2, and J3 increases by 49.42%, 49.04%, and 47.37%, respectively. The fracture shear stress of J1, J2, and J3 increases by 46.01%, 38.65%, and 38.71%, respectively. Under the partial anchorage condition, the peak shear stress of J1, J2, and J3 increases by 48.66%, 51.69%, and 49.45%, respectively. The fracture shear stress of J1, J2, and J3 increases by 50.00%, 40.00%, and 39.17%, respectively. It can be inferred that under the full-length anchorage condition, with the increase in normal stress, the increase in peak shear stress and fracture shear stress is less pronounced for rougher joint surfaces. Under the partial anchorage condition, with the increase in normal stress, the percentage increase in peak shear stress tends to increase, while the percentage increase in fracture shear stress tends to decrease

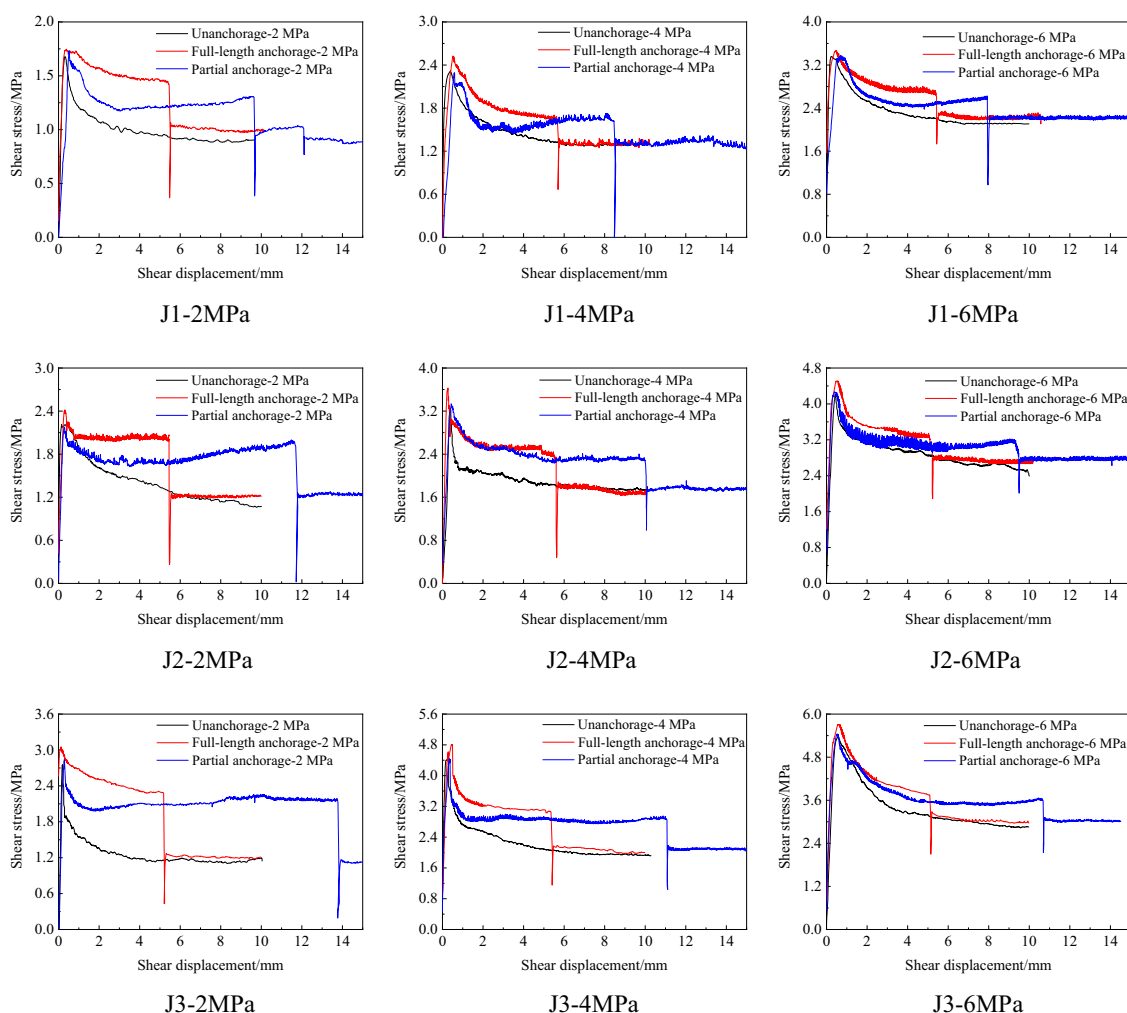


**Fig. 5** Shear stress–displacement curves

**Table 3** Peak shear stress and fracture shear stress of bolted joints under different conditions

Joint surface roughness	J1			J2			J3		
Normal stress/MPa	2.00	4.00	6.00	2.00	4.00	6.00	2.00	4.00	6.00
Peak shear stress for full-length anchorage case/MPa	1.75	2.51	3.46	2.40	3.60	4.71	3.00	4.80	5.70
Fracture shear stress for full-length anchorage case/MPa	1.42	1.65	2.63	2.00	2.40	3.26	2.28	3.00	3.72
Peak shear stress for partial anchorage case/MPa	1.72	2.29	3.35	2.15	3.30	4.45	2.75	4.42	5.44
Fracture shear stress for partial anchorage case /MPa	1.30	1.62	2.60	1.95	2.29	3.25	2.19	2.88	3.60

for rougher joint surfaces. This is related to the anchoring effect exerted by the bolts during the shearing process. Different conditions of joint surface roughness, normal stress, anchorage lengths, and shear displacement result in varying degrees of anchoring effects of the bolts, which lead to different magnitudes of increase in peak shear stress and fracture shear stress. Overall, it is indicated that the peak shear stress and fracture shear stress of bolted joints increases with an increase in normal stress or JRC, which is consistent with

the findings by Jiang et al. (2022), Wu et al. (2018b), and Chen et al (2018a).

It is important to note that according to Pellet et al. (1996), Spang et al. (1990), Maiolino et al. (2015), the effect of the joint dilatancy angle on the shear resistance force of the bolt increases with the bolt diameter. Therefore, the effect of the joint JRC on the shear resistance force of the bolt increases with the diameter of the bolt. In this paper, the diameter of the bolts is only 6 mm, which is smaller than



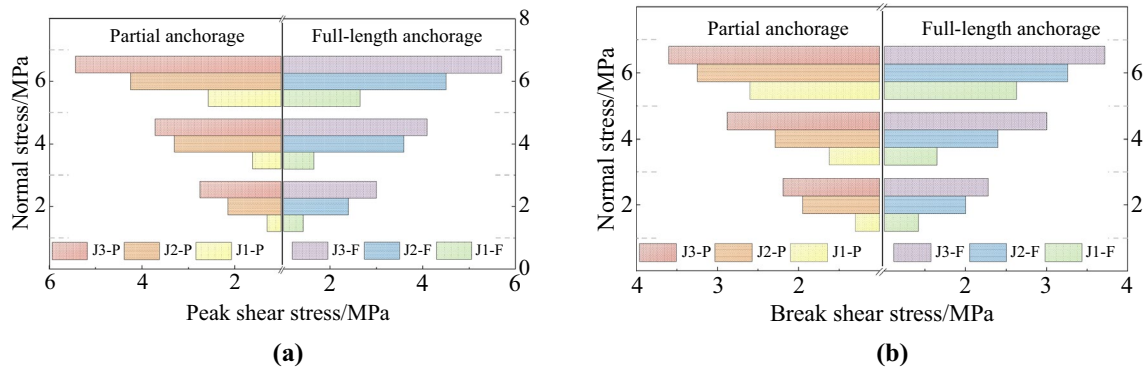


**Fig. 6** The peak shear strength and fracture shear stress of bolted joints under different normal stress conditions: **a** peak shear stress; **b** fracture shear stress

that of the field bolts. Therefore with the increase of JRC, the shear resistance force of the field bolts will increase more significantly.

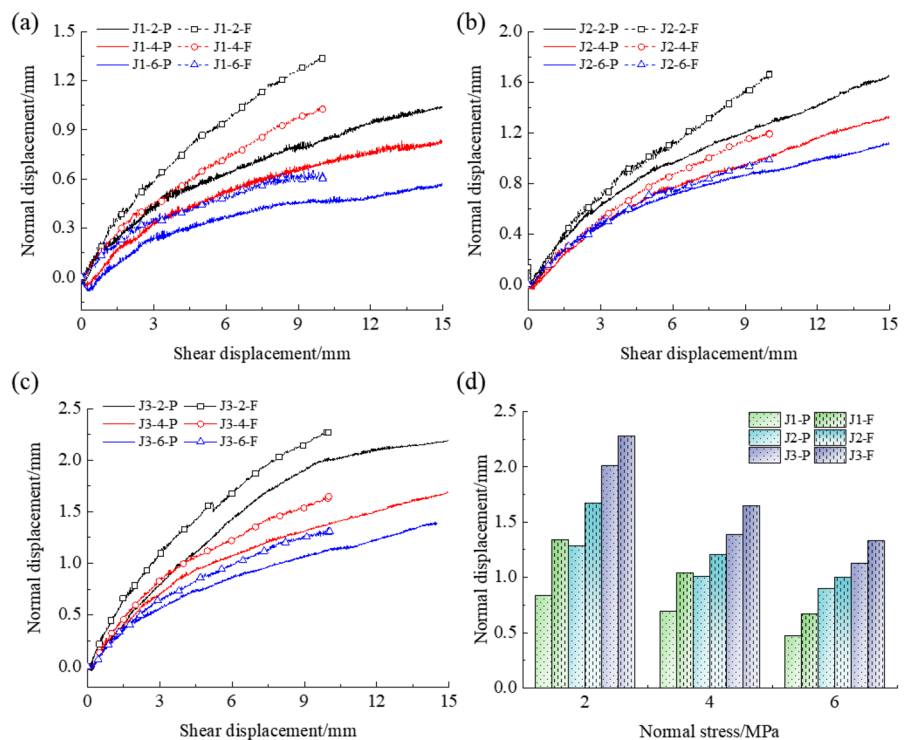
### 3.3 Shear Dilatancy Characteristic

Under different conditions, the normal displacement–shear displacement curves of bolted joints are presented in Fig. 7. As observed, both the normal displacement in partial anchorage and full-length anchorage cases exhibit non-linear increases with shear displacement. The slope of the normal displacement curve decreases gradually with the progress of shear. This phenomenon arises from the initial stages of

shear when the roughness of the joint surface remains intact; the rock blocks slide along the roughness, leading to a swift increase in normal displacement. With shear continuing, a significant portion of the roughness is disrupted, causing the blocks to move along the fractured roughness, resulting in a slower increase in normal displacement.

To analyze the impact of the anchorage length on joint shear dilation behavior, the shear dilation value was statistically determined at a 10 mm shear displacement (the maximum under the full-length anchorage), as depicted in Fig. 7d. In the partial anchorage, as the normal stress increases from 2 to 6 MPa, the shear dilation values of J1 decrease to 0.835, 0.688 and 0.474, a decrease of

**Fig. 7** The normal displacement–shear displacement curves of bolted joints under different conditions: **a** J1; **b** J2; **c** J3; **d** normal displacement when shear displacement at 10 mm



19.72%. The shear dilation values of J2 are 1.279, 1.006, and 0.898, respectively, which are reduced by 19.85%. The shear dilation values of J3 were 2.007, 1.388, and 1.128, respectively, a reduction of 25.83%. In the full-length anchorage, when the normal stress increases from 2 to 6 MPa, the shear dilation values of J1 are 1.341, 1.040, and 0.667, respectively, which are reduced by 22.45%. The shear dilation values of J2 are 1.665, 1.202, and 0.997, respectively, which are reduced by 27.79%. The shear dilation values of J3 are 2.278, 1.649, and 1.330, respectively, which are reduced by 27.61%. By comparing the normal displacement curves of partial anchorage and full-length anchorage cases, it is revealed that under the same conditions, the normal displacement in the partial anchorage configuration is lower than that in the full-length anchorage configuration. This difference is caused, because the partial anchorage effectively restrains the shear dilation behavior of the joint specimen. In the partial anchorage, since there is no grout in the free segment, the axial force of the bolt can be directly transmitted to the free end washer. The interaction between the washer and the rock specimen effectively restricts the shear dilation behavior of the joint, leading to a further increase in normal stress on the joint surface. In the full-length anchorage configuration, due to the confinement of the grout, the axial force of the bolt is mainly concentrated near the joint (Li et al. 2022c), and it cannot be fully transmitted. As a result, the restraining

effect on shear dilation behavior is not as pronounced as in the partial anchorage. Using a larger washer size will better promote the distribution of the axial force at the top of the rock sample, resulting in a more effective limitation of the joint dilatation behavior.

### 3.4 Damage Characteristic

#### 3.4.1 Joint Surface

Figure 8 illustrates the characteristics of joint surface damage. At the conclusion of the bolted joint shear test, substantial surface roughness near the bolt experienced significant damage. In addition, failure of the grout and surrounding rock near the bolt can be observed due to compression of the bolt in the shear direction. To analyze the damage and failure characteristics of the joint surface, image processing was conducted on the joint surface after shear tests, as shown in Fig. 8. The specific image processing method involved the following steps: First, the damaged portions of the joint surface were selected as the feature range. Then, based on this range, similar areas were selected. Finally, all the damaged areas on the joint surface were identified and highlighted (shown as white areas within red circles in the image). The principle is that the color and brightness of the joint surface change after damage occurs. Therefore, in image processing software, the grayscale range of the damaged area can be

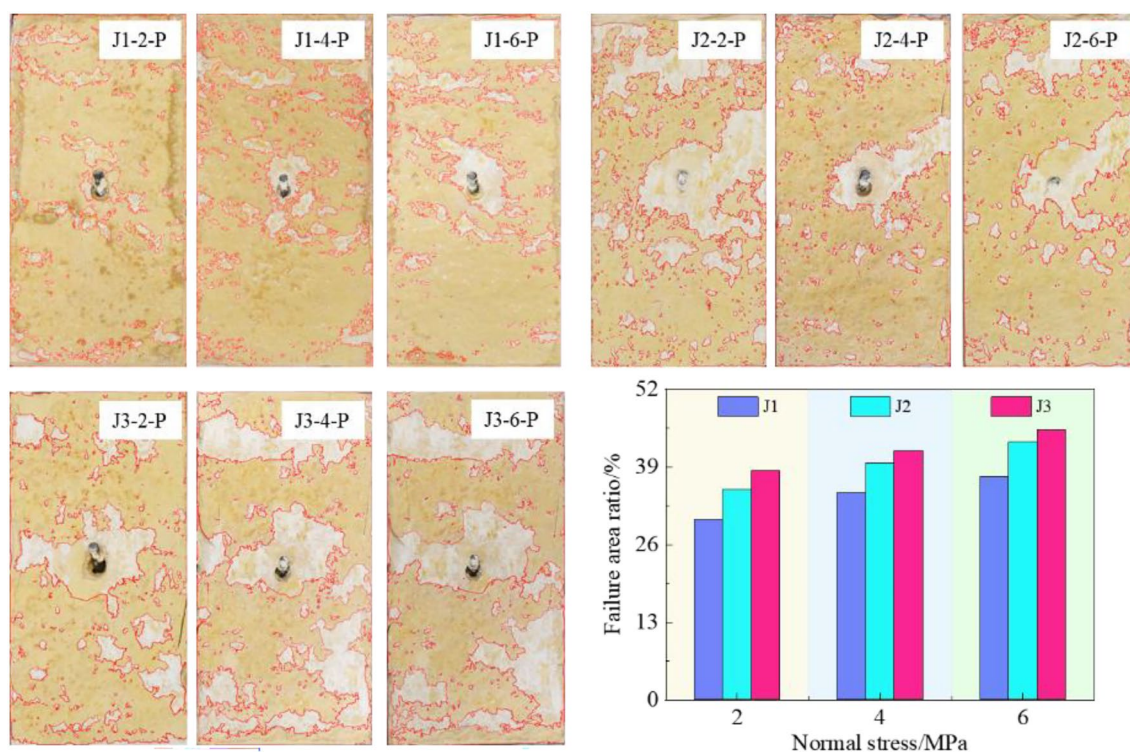


**Fig. 8** The patterns of fracture surface damage under various conditions of normal stress and Joint Roughness Coefficient (JRC)

defined as the feature value range. Subsequently, this range is used to identify the entire damaged area in the image. Research indicates that joint surface roughness and normal stress are the primary factors influencing the extent and area of damage on the joint surface (Jiang et al. 2022; Grasselli et al. 2002). In this section, the experimental results under the partial anchorage are selected as an example for analysis. To assess the influence of normal stress and Joint Roughness Coefficient (JRC) on the joint surface damage characteristics, the damaged areas on the joint specimen surfaces were quantified. For the J1 specimen, the ratios of damaged area were 30.12%, 34.61%, and 37.27% under normal stresses of 2 MPa, 4 MPa, and 6 MPa, respectively. Similarly, for the J2 specimen, the ratios were 35.17%, 39.55%, and 43.11%, and for the J3 specimen, the ratios were 38.25%, 41.64%, and 45.13%.

This analysis shows that under the same JRC condition, an increase in normal stress leads to an increase in the extent of joint surface damage. However, the location of damage on the joint surface remains relatively consistent. This can be attributed to the fact that the angles of the rough elements on the rough joint surface determine the contact characteristics during shearing. Grasselli et al. (2002) have suggested that the potential contact area of a joint is related to the angles of the rough elements on the joint surface, and that the contact area can be simplified to only consider the region facing

the shearing direction and having an angle larger than the critical viewing angle. Similarly, due to different levels of joint surface roughness, the extent of damage on the joint surface varies for different JRC values under the same normal stress conditions. The analysis also reveals that, under the same normal stress, higher JRC values correspond to larger areas of joint surface damage. This is attributed to the fact that a rougher joint surface with a more complex distribution of angles and larger surface area has a larger initial contact area during shearing, leading to a larger area of damage on the joint surface.

To assess the influence of different anchorage lengths on the joint surface damage characteristics, the results of the J2 joint are taken as an example to analyze the damaged areas on the joint specimen surface for both the partial anchorage and full-length anchorage, as shown in Fig. 9. When the normal stress is 2 MPa, 4 MPa, and 6 MPa, the ratios of damaged area for the J2 joint under the partial anchorage are 35.17%, 39.55%, and 43.11%, respectively. For the full-length anchorage, the ratios are 10.95%, 12.38%, and 15.79%. For the unanchorage, the ratios are 5.94%, 7.74%, and 12.39%. Comparing the above data, it is evident that under the partial anchorage, the extent of joint surface damage is larger. This is attributed to two main reasons: first, the total shear displacement under the partial anchorage is greater than under the full-length anchorage, meaning that

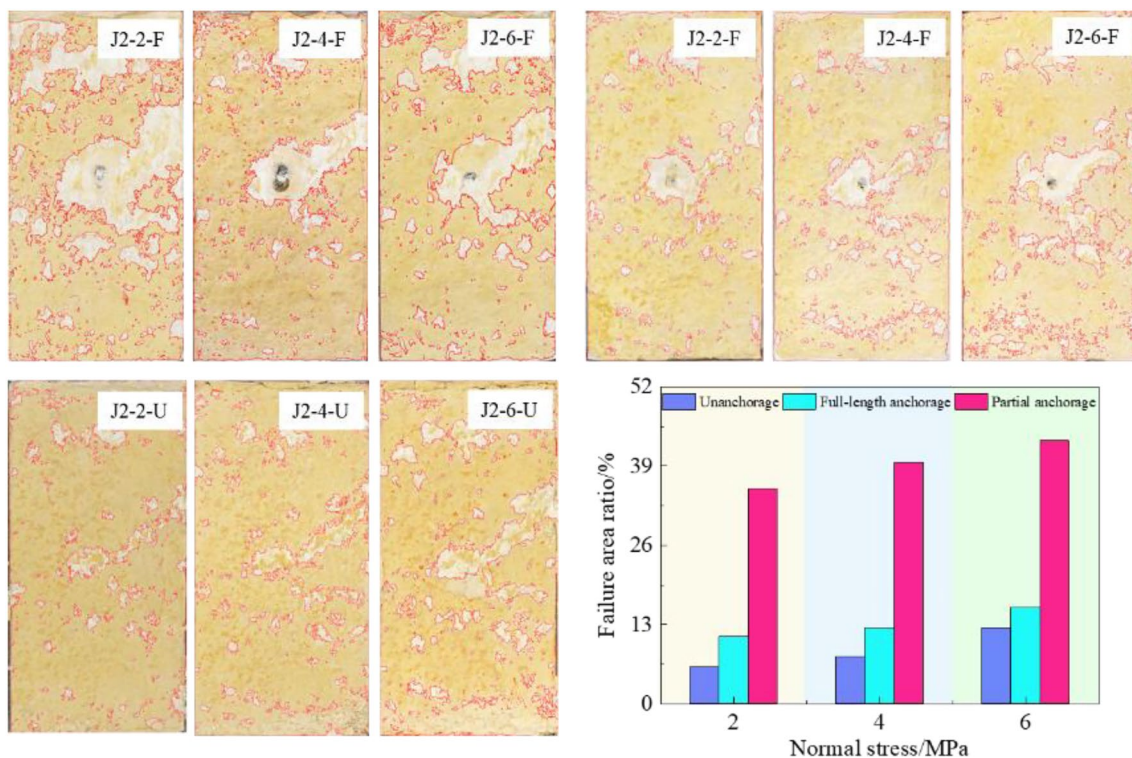


Fig. 9 The fracture patterns on the joint surfaces under distinct conditions of anchorage lengths

the joint surface under partial anchorage experiences longer periods of shearing displacement. However, this is not the main reason. According to reference (Chen et al. 2018b), the damage on the fracture surface mainly occurs near the peak shear displacement (shear displacement not exceeding 1 mm), and less damage occurs within the residual stage (shear displacement exceeding 5 mm). Similarly, in the process of anchor joint shearing, the damage on the fracture surface mainly occurs before the bolt breaks, and less damage occurs after the bolt breaks; This is detailed in Sect. 4.1. Therefore, accurately speaking, one reason is due to the larger bolt breaking displacement in the case of partial anchorage compared to full-length anchorage; the second reason is that in partial anchorage, there is no restriction from grout on the bolt, making it easier for the axial force of the bolt to be transmitted, which increases the normal stress on the fracture surface. Although full-length anchorage also increases the normal stress on the fracture surface, it is mainly concentrated in a small range where the bolt intersects with the fracture. Overall, the reason for the fracture surface damage area is larger in the case of partial anchorage is that the axial force of the bolt can be more effectively transmitted, effectively increasing the normal stress on the fracture surface, and the breaking shear displacement in partial anchorage is longer, leading to a longer duration of action on the fracture surface.

### 3.4.2 Bolt

To analyze the deformation and failure characteristics of bolts under different conditions, the bolts were removed from the specimens after the shear tests and photographed, as shown in Fig. 10 (the yellow lines indicate the fracture section of the bolt); it can be observed that the deformation of the bolt is mainly concentrated near the joint surfaces, and after shear failure, it exhibits a generally “S”-shaped deformation pattern. Under the full-length anchorage condition, the bolt deformation is mostly symmetric around the center, while under the partial anchorage condition, the deformation is asymmetric. Overall, the deformation of the bolt is greater under the partial anchorage condition compared to the full-length anchorage condition. The fracture characteristics of the bolts in the figure indicate that the bolt fractures into two or three segments, which is consistent with the experimental results of Wu et al. (2018a). The occurrence of fracture into different segments is mainly influenced by the fracture position of the bolt and the roughness of the joint surfaces. Jalalifar et al. (2010) have pointed out that the fracture of the bolt may occur at the location of maximum bending moment (plastic hinge) or at the intersection of the bolt and the structural surface. When the fracture position of the bolt occurs at the plastic hinge, one end of the broken bolt will still protrude from the joint surface. Under the action of normal

stress, on one hand, the protruding end of the broken bolt will be partially embedded into the rock due to compression, limiting the sliding of the bolt; on the other hand, it will cause a significant tensile stress on one side of the plastic hinge of the bolt. The combined effect of these two factors results in a secondary fracture of the bolt.

Figure 10 shows distinct fracture characteristics indicating two primary failure modes: flexural-tension and flexural-shear failures (Fig. 10c). The figure illustrates that in flexure-tension failure, the bolt undergoes a greater deformation range than in flexure-shear failure. In flexure-tension failure, fractures predominantly occur at or near the point of maximum bending moment, commonly near the plastic hinge. The angle between the fracture normal and the shear direction is usually below  $90^\circ$ . In flexure-shear damage, fractures occur at the point of maximum shear stress, where the angle between the fracture normal and shear direction exceeds  $90^\circ$ .

From Fig. 10, it can also be observed that under the full-length anchorage, as the normal stress and JRC increase, the deformation range of the bolts decreases. This is attributed to the presence of grout in the full-length anchorage, which restricts the axial load transfer of the bolts. As a result, the deformation and stress concentration of the bolts mainly occur near the joint surfaces, further influenced by the surface morphology of the joint where the bolts are installed. Under the partial anchorage, with the increase of normal stress, the overall deformation range of the bolt tends to decrease, while with the increase of JRC, the deformation range of the bolt generally increases. This is mainly due to the fact that in the partial anchorage, the bolt does not initially contact the surrounding rock. Significant bending deformation of the bolt occurs only after contact with the surrounding rock. Thus, the position of contact between the bolt and the surrounding rock determines the deformation range of the bolt. It is well known that with an increase in normal stress or a decrease in JRC, joint dilation decreases (Wang et al. 2022). Consequently, as the normal stress increases and joint dilation decreases, the deformation range of the bolt decreases when it comes into contact with the surrounding rock. Similarly, with an increase in JRC and corresponding joint dilation, the deformation range of the bolt increases.

The study aimed to quantitatively analyze bolt deformation by recording displacements at the bolt failure point under varied conditions, as depicted in Fig. 11. In the figure ‘ $D_b$ ’ represents the shear displacement with ‘ $D_{bF}$ ’ for full-length anchorage and ‘ $D_{bP}$ ’ for partial anchorage. ‘ $D_{bP}$ ’ notably surpasses ‘ $D_{bF}$ ’ in Fig. 11, indicating that in the partial anchorage, the bolt’s fracture shear displacement is significantly influenced by normal stress and joint surface roughness. In addition, Fig. 13 shows that under the partial anchorage, as the normal stress increases from 2 to 6 MPa,

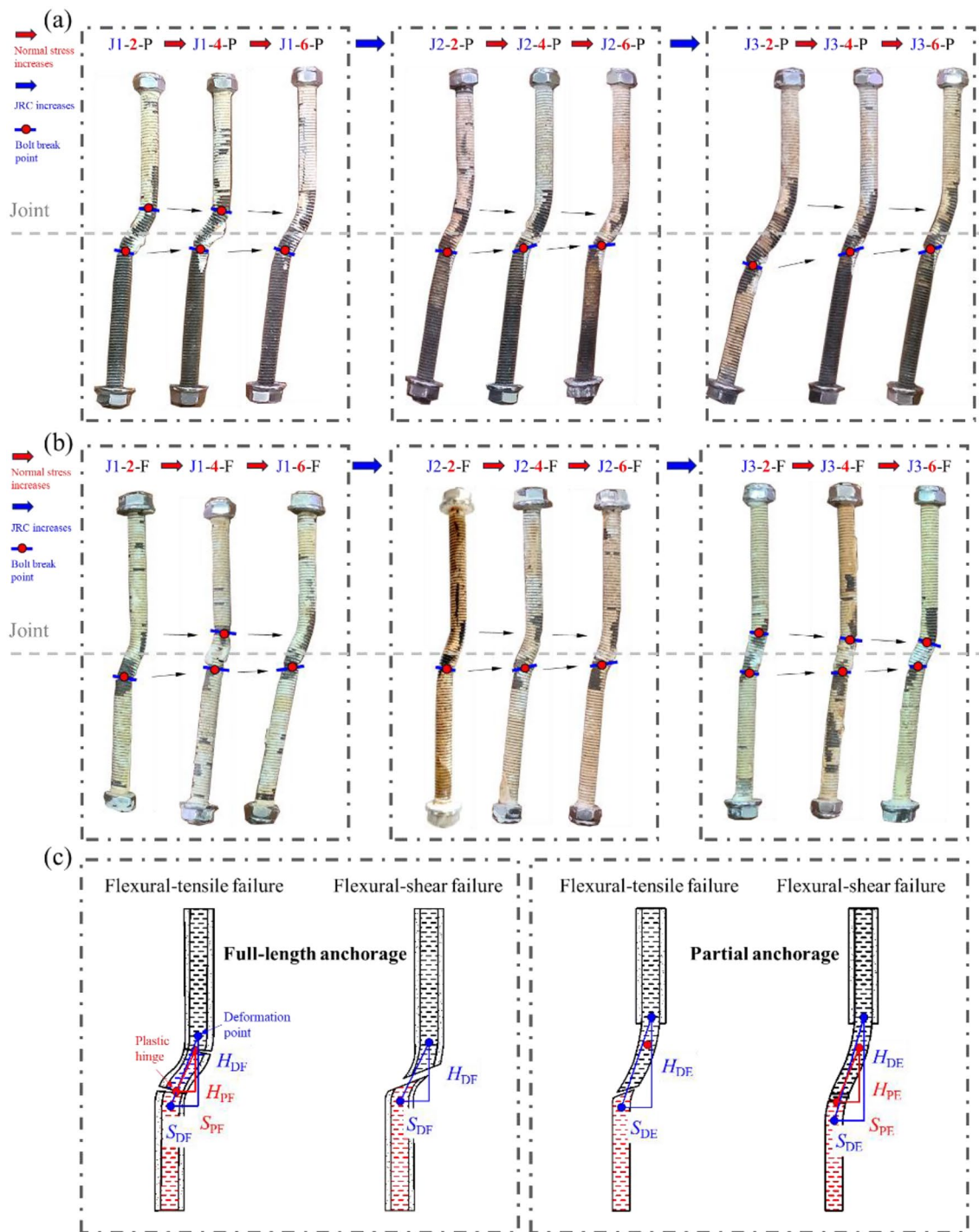
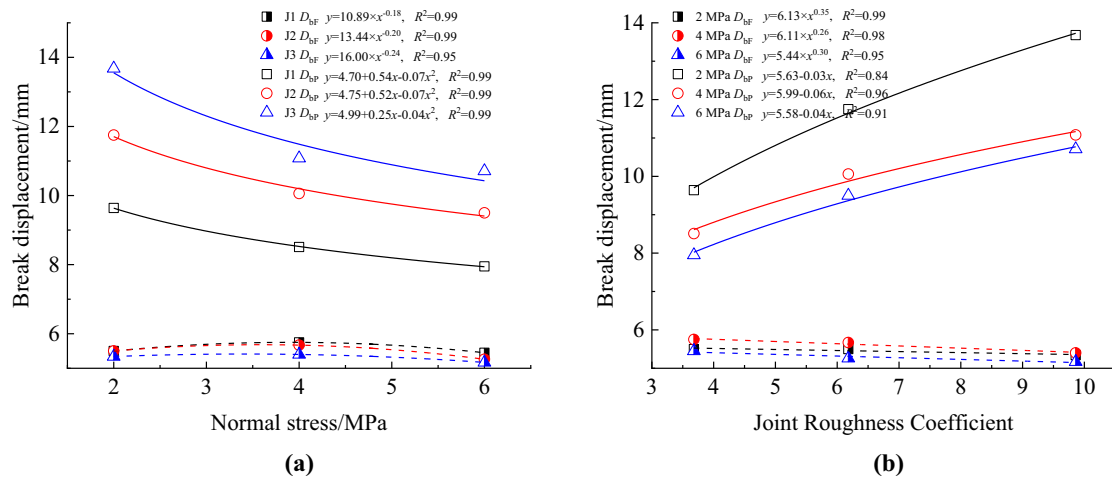


Fig. 10 Failure diagram of bolt deformation: **a** partial anchorage; **b** full-length anchorage; **c** schematic diagram of broken bolt

the fracture shear displacements for ‘J1’ were 9.64, 8.51, and 7.95, respectively, a reduction of 17.53%. The fracture shear displacements for ‘J2’ were 11.75, 10.06, and 9.50, respectively, a reduction of 19.15%. The fracture shear displacements for ‘J3’ were 13.68, 11.08, and 10.7 respectively, a reduction of 21.71%. Under the full-length anchorage, as

the normal stress increases from 2 to 6 MPa, the fracture shear displacements for ‘J1’ were 5.50, 5.75, and 5.45, respectively, a reduction of 0.91%. The fracture shear displacements for ‘J2’ were 5.50, 5.67, and 5.26, respectively, a reduction of 4.36%. The fracture shear displacements for ‘J3’ were 5.34, 5.40, and 5.17, respectively, a reduction of



**Fig. 11** The bolt shear fracture displacement under different conditions of normal stresses and various Joint Roughness Coefficient (JRC): **a** various normal stress; **b** various JRC; **c** schematic diagram of fractured bolt

3.18%. From the aforementioned data, it is evident that with the increase in normal stress, the ‘ $D_{bp}$ ’ curve displays a non-linear reduction, while the ‘ $D_{bf}$ ’ curve initially increases before decreasing, exhibiting an overall decreasing trend.

## 4 Shear Performance of Bolt

### 4.1 Evolutionary Patterns of Anchoring Effects of Bolt

As analyzed in Sect. 3.1, continuous shear results in shear stress curves for both partial anchorage and full-length anchorage configurations that are notably higher than that for the unanchored condition. This indicates that anchor bolts continuously exert their anchoring effects during the shearing process, until the anchor bolts fracture. From Fig. 4, it can be observed that during the shearing process, the anchoring effects of partial anchorage and full-length anchorage anchor bolts differ; To quantitatively analyze the shear resistance provided by anchor bolts under different anchorage lengths, the shear stress of the full-length anchorage configuration is subtracted from the shear stress of the partial anchorage configuration under the same shear displacement conditions, yielding the difference of shear stress (DSS) between the two anchorage lengths, as shown in Fig. 12a. The DSS for the three types of rough bolted joint specimens (J1, J2, and J3) under different normal stress conditions are presented in Fig. 12b–d.

It is evident that the variation trends of the DSS curves for different rough bolted joints under various normal stress conditions are consistent. As the shear process progresses, the DSS curves generally exhibit five stages:

Stage ① (Corresponding to part I<sub>p</sub> of the shear stress curve): From the onset of shearing to around the maximum peak of shear displacement (the largest peak shear displacement among both full-length anchorage and partial anchorage), the DSS increases and then decreases with shear displacement. This is because in the full-length anchorage configuration, the “pin effect” is more quickly employed, rapidly mobilizing the shear stress of the anchor bolt. As shear displacement increases, the shear stress mobilized by the anchor bolt is greater. Conversely, in the partial anchorage configuration, without the presence of grouts, the anchor bolt does not exert the “pin effect”. Therefore, under the same shear displacement conditions, the shear stress in the partial anchorage configuration is lower than in the full-length anchorage configuration. Moreover, as shearing progresses, the difference in shear stress between full-length anchorage and partial anchorage configurations increases. When the shear stress of the full-length anchorage reaches its peak, the shear stress of the partial anchorage has not yet reached its peak. Consequently, in the subsequent shearing process, the shear stress of the full-length anchorage starts to decrease, while the shear stress of the partial anchorage continues to increase, causing the DSS to rapidly drop and even become negative.

Stage ② (Corresponding to part II<sub>p</sub> of the shear stress curve): involves moving to the maximum peak of shear displacement until the bolt comes into contact with the surrounding rock (partial anchorage configuration). During this stage, the DSS curve starts to rise gradually; this is due to the fact that in the end, the bolt and surrounding rock have not yet made contact, so that the shear stress curve for partial anchorage decreases rapidly. In contrast, with the full-length anchorage, the shear stress curve declines slowly due

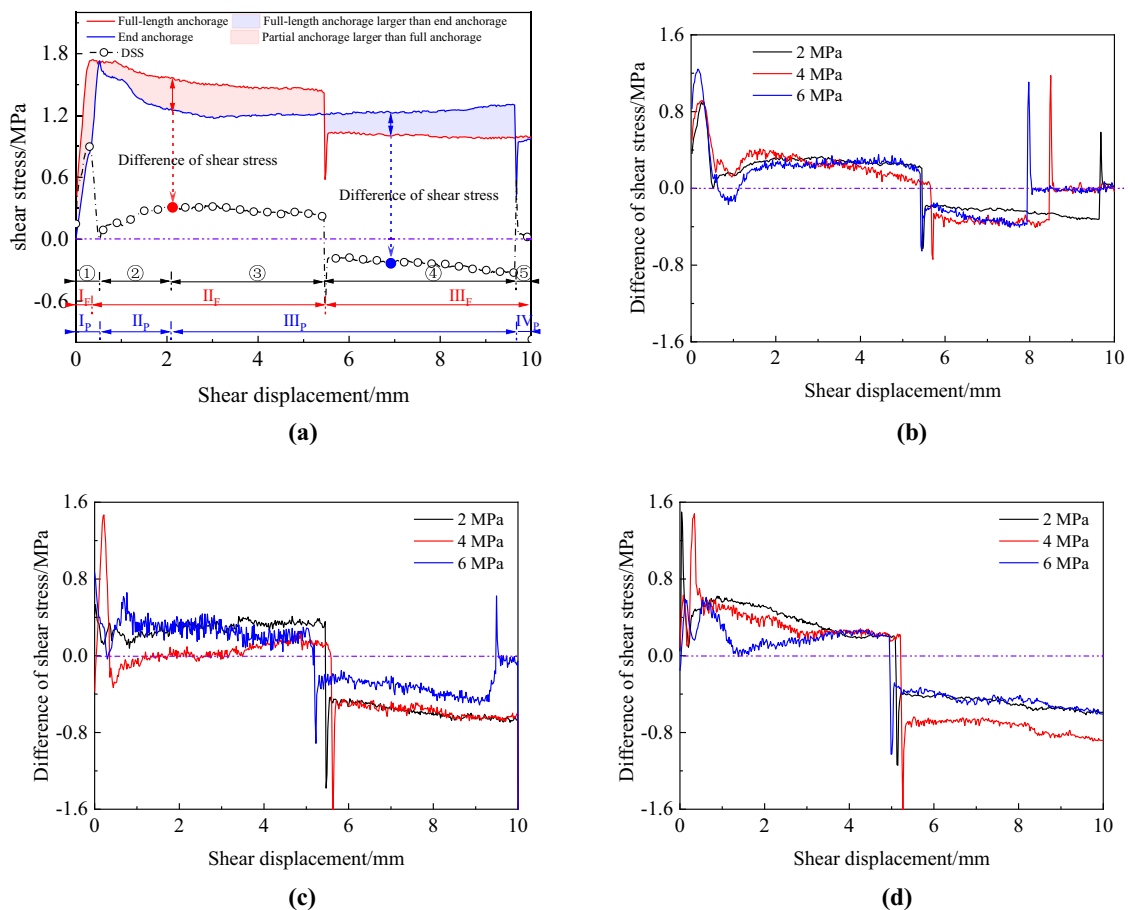


Fig. 12 Difference in shear stress: **a** difference in shear stress; **b** J1; **c** J2; **d** J2

to the shear resistance provided by the bolt, leading to a slow increase in DSS again.

Stage ③ (Corresponding to the overlap of  $II_F$  and  $III_P$  in the shear stress curve): encompasses the period from when the bolt contacts the surrounding rock (partial anchorage) to the complete failure of the full bolt. DSS remains relatively constant during this stage. The partial anchorage causes the bolt to swiftly exert its “pinning effect” on the surrounding rock upon contact, causing the shear stress curve for partial anchorage to stop decreasing and begin to rise slowly. As a result, the DSS curve remains relatively stable throughout this stage.

Stage ④ (Corresponding to the remainder of  $III_P$  in the shear stress curve): as the displacement shifts from full bolt failure to end bolt failure, the DSS curve abruptly drops to negative values and then starts decreasing gradually. This is because in the full anchor method, the shear stress from the bolt rapidly drops upon failure, falling below the shear stress of the partial anchorage. Furthermore, since the bolt in the partial anchorage has not fractured, its shear stress continues

to increase slowly. Consequently, the DSS becomes negative and decreases continuously.

Stage ⑤ (Corresponding to part  $IV_P$  of the shear stress curve): from end bolt failure to a shear displacement of 10 mm, DSS remains close to 0. After the failure of the bolt, the shear strength of the anchor joint primarily relies on the joint surface, independent of the anchorage length.

From Fig. 12, it can also be observed that under the same rough joint conditions, as the normal stress increases, the overall DSS curves show minimal variation. This effect is especially pronounced when the joint roughness is relatively small; For instance, the DSS curves for the J1 bolted joint specimen closely align across the three different normal stress conditions.

## 4.2 The Improved Shear Stress of Bolt

To measure the enhancement effect of bolts on joint shear strength, previous studies (Jiang et al. 2022); commonly defined the shear stress decrease upon bolt failure as the bolt enhanced shear stress, denoted as  $T_2$ . Therefore, to

analyze the enhancement effects of the partial anchorage and full-length anchorage on joint shear strength, this study collected the bolt enhanced shear stress  $T_{2F}$  under the full-length anchorage, as well as the bolt enhanced shear stress  $T_{2E}$  under the partial anchorage, as shown in Fig. 4.

The statistical analysis of  $T_2$  under the two anchorage lengths was conducted, and the results are presented in Fig. 13; it is evident that the specific anchoring effects of the bolts vary based on the anchorage method: Under J1 joint conditions, with normal stresses of 2 MPa, 4 MPa, and 6 MPa, values of  $T_{2F}$  are 0.42 MPa, 0.35 MPa, and 0.33 MPa, respectively, while values of  $T_{2E}$  are 0.38 MPa, 0.32 MPa, and 0.3 MPa. Under J2 joint conditions, with normal stresses of 2 MPa, 4 MPa, and 6 MPa, values of  $T_{2F}$  are 0.83 MPa, 0.60 MPa, and 0.49 MPa respectively, while values of  $T_{2E}$  are 0.75 MPa, 0.54 MPa, and 0.45 MPa. Under J3 joint conditions, with normal stresses of 2 MPa, 4 MPa, and 6 MPa, values of  $T_{2F}$  are 1.04 MPa, 0.85 MPa, and 0.64 MPa, respectively, while values of  $T_{2E}$  are 0.98 MPa, 0.80 MPa, and 0.59 MPa.

Based on the data above, it can be observed that  $T_2$  are generally larger under the full-length anchorage compared to the partial anchorage. However, the difference between the two methods is not substantial, ranging from approximately 0.03 to 0.08 MPa. This indicates that the full-length anchorage method provides a better enhancement in joint shear strength compared to the partial anchorage, but the improvement is limited. This is because, at the point of ultimate failure of the anchorage system, the bolt is the primary load-bearing structure. Consequently, the fracture shear stress is primarily determined by the shear strength of the bolt itself, resulting in a minimal difference in fracture shear stress between the two anchorage conditions.

It is evident that both the full-length anchorage and partial anchorage show the following patterns: 1. Under the same normal stress conditions, as the JRC increases, the bolt enhanced shear stress  $T_2$  also increases. 2. Under the same JRC, as the normal stress increases, the bolt enhanced shear stress  $T_2$  decreases. This behavior can be attributed to the formation of a pair of symmetrically distributed plastic hinges near the joint during the shearing process. Once these plastic hinges form, the bolt undergoes shear yielding. After shear yielding, in subsequent shear processes, the bolt exhibits mechanical properties similar to a truss member, meaning that shear forces remain constant, while axial forces gradually increase. With the increase in axial force, the axial strain of the bolt gradually increases until it experiences tensile failure (Chen et al 2018b; Ma et al. 2019).

Based on this analysis, the enhancement effect of bolts on joint shear strength is highly dependent on the axial force acting on the bolt. When the normal stress on the joint is high, the axial deformation of the bolt is relatively small, making it difficult to engage the axial force of the bolt. As

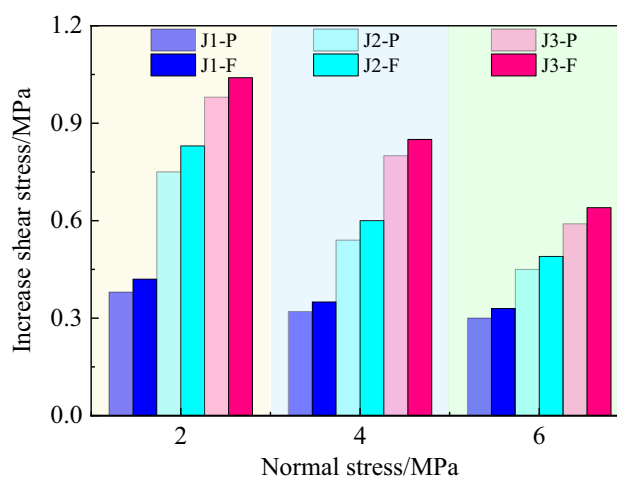


**Fig. 13** The bolt enhanced shear stress under different normal stress and JRC

a result, the shear resistance provided by the bolt gradually weakens as the normal stress increases. On the other hand, as JRC increases, it leads to increased shear dilation deformation of the joint, which in turn induces elongation deformation in the bolt. This mobilizes the axial force of the bolt to provide shear resistance, causing the shear resistance offered by the bolt to increase as JRC increases.

## 5 Shear Acoustic Emission Characteristics of Bolted Joints

### 5.1 Hit and Energy

During the rock failure process, the acoustic emission signals released contain vital information about the rock failure mechanism. Hit represents the number of acoustic emission events within a specified time period, indicating the activity level of fracture initiation and propagation within the material. Energy quantifies the total energy released during these acoustic emission events, reflecting both the rate and intensity of fracture expansion in the material. Therefore, in the previous studies, (Meng et al. 2019; Zhang et al. 2020a, b; Liu et al. 2022) have extensively employed acoustic emission parameters (Hit and Energy) to assess microfracture quantities and magnitude in rock joints during shearing, effectively unveiling the evolutionary damage process in these joints. It can provide a research basis for the prediction method of the roadway surrounding rock state and the accurate prediction in the engineering field. This chapter combines acoustic emission techniques to analyze the influence of different normal stresses, Joint Roughness Coefficients (JRC), and anchor methods on the damage evolution patterns of bolted joints. Only the results for cases, such as J2-2-E,



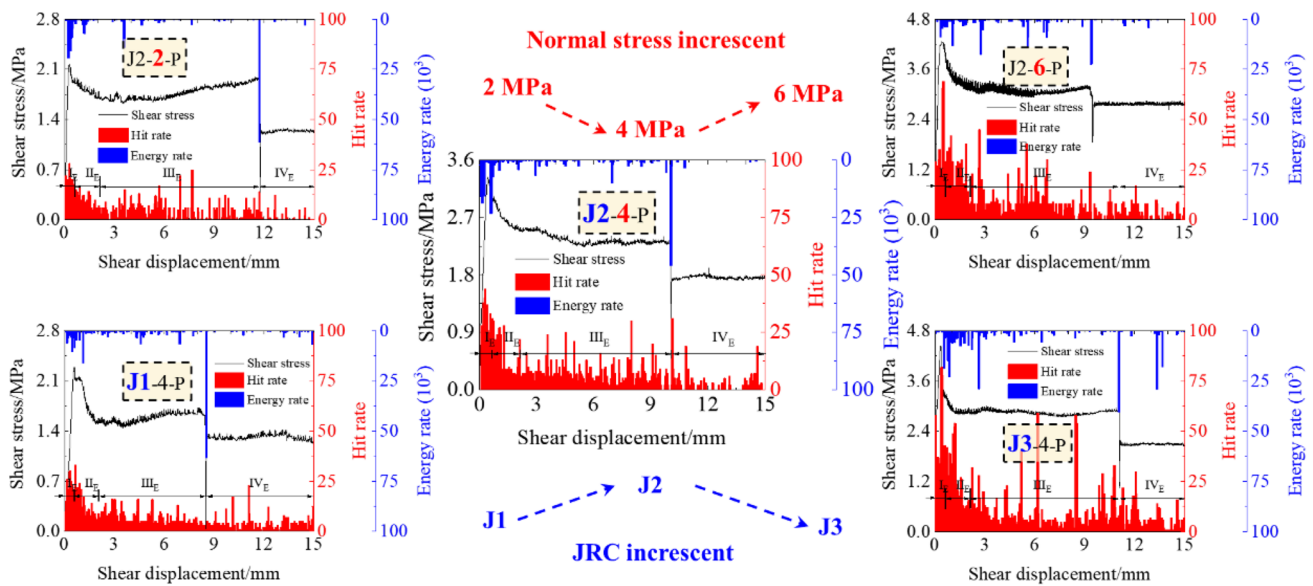


Fig. 14 The variation characteristics of acoustic emission characteristic parameters under the partial anchorage

J2-4-E, J2-6-E, J1-4-E, J3-4-E, and J2-2-F, J2-4-F, J2-6-F, J1-4-F, and J3-4-F, are presented for analysis. Figures 14 and 15 display the monitoring results of the acoustic emission characteristic parameters Hit rate and Energy rate under the partial anchorage and full-length anchorage, respectively.

The main task of this study is to investigate the relationship between the shear behavior of bolted joints and the acoustic emission characteristics. At different stages of the shearing process of bolted joints, the acoustic emission characteristics are different. From Fig. 14, it can be observed that under the partial anchorage: In Stage

$I_E$ , the Hit rate increases continuously until reaching its maximum value. This is because, at the start of shearing, most of the asperities on the joint surface undergo primarily elastic deformation without significant damage, and only a small portion experiences damage and friction. As shearing continues, at the instant when the shear stress peaks, a large number of asperities are torn apart. In Stage  $II_E$ , the Hit rate decreases steadily. This is due to during Stage  $I_E$ , a substantial number of asperities have already been damaged. The number of asperities undergoing damage decreases in this stage. Additionally, fragments of asperities

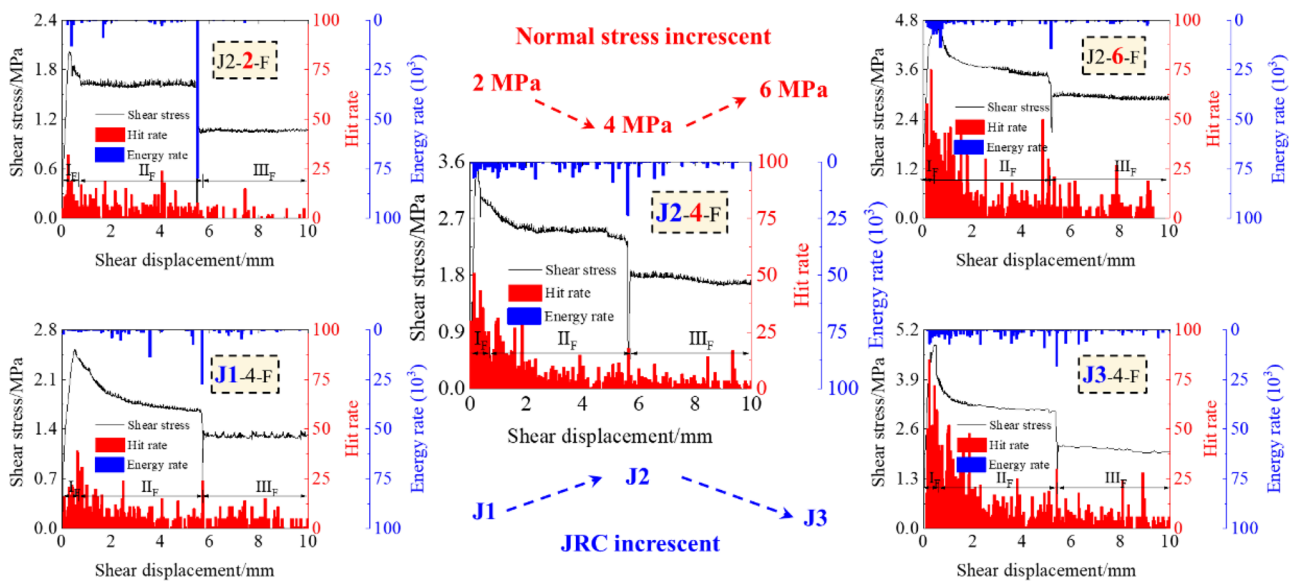


Fig. 15 The variation characteristics of acoustic emission characteristic parameters under the full-length anchorage

that were torn apart in Stage I<sub>E</sub> remain within the joint and are subjected to secondary grinding during the shearing process. Hence, while the Hit rate decreases in Stage II<sub>E</sub>, it still remains relatively high overall. In Stage III<sub>E</sub>, the Hit rate is relatively low and stable. This is because, during this stage, there is minimal further damage to asperities. Acoustic emission impact signals are primarily generated by friction between the joint surfaces. It needs to be noted that within this stage, certain instances of a sudden increase in the Hit rate occur. This can be attributed to two factors: First, as shearing progresses, the contact area of the joint surface continually reduces, causing stress concentration on the asperities. Consequently, under high concentrated stress, slight failures occur in the asperities, leading to acoustic emission signals. Second, within this stage, the bolt comes into contact with the surrounding rock, resulting in mutual compression. This can cause rock damage, especially when approaching the bolt failure, leading to an increase in the Hit rate. In Stage IV<sub>E</sub>, the Hit rate continues to decrease further. In this stage, the Hit rate is primarily generated by two factors: friction between the joint surfaces and friction between the failed bolt and the joint. As analyzed in Sect. 3.4, after the bolt failures, a portion remains higher than the joint surface. Therefore, this segment of the bolt continues to interact with the joint surface, generating a small amount of acoustic emission signals.

From Fig. 14, it is found that the Energy rate shows a similar changing trend to the Hit rate in different stages: In Stage I<sub>E</sub>, the Energy rate starts increasing continuously. Upon entering Stage II<sub>E</sub>, it begins to decrease steadily. In Stage III<sub>E</sub>, the Energy rate notably decreases, which is due to the predominance of friction on the joint surface during this stage, resulting in smaller acoustic emission energy. Similarly, individual instances of a sudden increase in Energy rate indicate micro-fractures occurring on the joint surface or near the bolt; Especially during bolt failure, the Energy rate increases significantly and surpasses the Energy rate value at the shear stress peak. This signifies that the energy released upon bolt failure is far greater than the energy produced during asperity damage on the joint surface. In Stage IV<sub>E</sub>, the Energy rate remains at a relatively low level; Occasional sharp increases indicate moments of fracture occurrence under concentrated stress or interaction between the failure bolt and the joint surface. Overall, the changing pattern of Energy rate closely mirrors that of Hit rate in various stages. From Fig. 15, it is apparent that under the full-length anchorage, the evolution patterns of Hit rate and Energy rate are generally similar to those under the partial anchorage. However, the difference is that under the full-length anchorage, the acoustic emission signals within a certain distance after the peak are higher compared to the partial anchorage. This indicates that within this distance after the peak, during the early shearing phase,

the interaction between the bolt and the surrounding rock is more intense under the full-length anchorage compared to the partial anchorage, highlighting a stronger anchoring effect of the bolt.

Based on the acoustic emission monitoring data, under the partial anchorage, when the normal stress is 2 MPa, 4 MPa, and 6 MPa, the corresponding maximum Hit rates are 28, 40, and 68, and the maximum Energy rates are  $61.414 \times 10^3$ ,  $46.015 \times 10^3$ , and  $22.454 \times 10^3$ , respectively. The cumulative Hit counts are  $2.717 \times 10^3$ ,  $3.965 \times 10^3$ , and  $4.782 \times 10^3$ , and the cumulative Energy are  $20.347 \times 10^4$ ,  $29.507 \times 10^4$ , and  $22.944 \times 10^4$ . This reveals that under the partial anchorage, with the same JRC, as the normal stress increases, the maximum Hit rate and cumulative Hit count increase. This is due to the fact that with higher normal stress, more asperities on the joint surface are damaged at the shear stress peak. As the normal stress increases, the maximum acoustic emission energy decreases. As analyzed in Sect. 3.4, the deformation range of the bolt generally decreases with increasing normal stress. Therefore, the accumulated deformation energy of the bolt becomes smaller, leading to a reduction in the energy released upon bolt failure. Furthermore, with increasing normal stress, the cumulative energy first increases and then decreases. This is because, as the normal stress on the joint surface increases, the concentrated stress on the asperities becomes larger, resulting in more significant energy release during asperity damage. However, as the energy released upon bolt failure decreases, it leads to fluctuations in the cumulative energy. Under the full-length anchorage, as the normal stress increases from 2 to 6 MPa, the corresponding maximum Hit rates exhibit an upward trend to be 32, 51, and 75, respectively. Simultaneously, the maximum Energy rates display a declining pattern of becoming  $79.556 \times 10^3$ ,  $23.603 \times 10^3$ , and  $14.493 \times 10^3$ , respectively. With respect to the cumulative counts, they present values of  $1.270 \times 10^3$ ,  $3.140 \times 10^3$ , and  $4.635 \times 10^3$  for Hits, and  $13.495 \times 10^4$ ,  $28.203 \times 10^4$ , and  $19.928 \times 10^4$  for Energy, respectively. It is indicated that under the full-length anchorage and identical JRC, the rise in normal stress leads to proportional increments in both the maximum Hit rate and cumulative Hit count, whose reason aligns with the aforementioned rationale. Furthermore, the increase in normal stress results in a reduction in the maximum emitted acoustic energy, indicating overall decreasing trend in deformation range of the bolt. This correlation corresponds with the findings discussed in Sect. 3.4. Moreover, as the normal stress increases, the cumulative energy initially increases and subsequently decreases. This phenomenon is attributed to the amplified concentrated stress on the rough surfaces of the joint plane with an increase in normal stress. Consequently, higher energy is released upon the failure of the rough surfaces, while the energy associated with the fracture of the bolt decreases, causing fluctuations in the cumulative energy. From these insights, it can be deduced that under

the same normal stress and JRC conditions, the full-length anchorage yields a larger maximum Hit rate compared to the partial anchorage, suggesting that the full-length anchorage generates more damage at the shear stress peak, this owes to the quicker interaction between the bolt and the surrounding rock. The energy release data further support this notion, as the full-length anchorage results in an overall decrease in maximum energy, indicating a smaller deformation range of the bolt compared to the partial anchorage, which aligns with the observations made in Sect. 3.4.

## 5.2 AE $b$ Value

The  $b$  of acoustic emission can serve as a characteristic value to describe the relative proportion of small-magnitude and large-magnitude events. A high  $b$  for acoustic emission corresponds to a significant number of low-intensity acoustic emission events, while a low  $b$  corresponds to a rapid increase in large cracks and an accelerated crack propagation rate. An increase in the  $b$  of acoustic emission indicates enhanced acoustic emission activity during the rock loading process, primarily manifesting as small-scale microcracks. Conversely, a decrease in the  $b$  indicates a reduction in the number of acoustic emission events during loading, accompanied by the emergence of large-scale cracks or a sharp increase in crack propagation rate (Ma et al. 2023). This illustrates that the evolutionary pattern of the  $b$  for acoustic emission holds crucial guidance for a profound understanding of rock failure mechanisms and the prevention of disaster incidents caused by the instability resulting from rock failure (Meng et al. 2019; Zhang et al. 2017).

In 1944, Gutenberg and Richter (1944) proposed a significant seismic frequency–magnitude ( $F$ – $M$ ) law, with the following expression:

$$\log_{10} N = a - bM, \quad (6)$$

where  $M$  represents the seismic magnitude;  $N$  denotes the cumulative frequency of seismic events with magnitudes greater than  $M$ ;  $a$  and  $b$  are two constants.

The calculation of  $b$  for acoustic emission follows the same method as that for seismic  $b$  value (Zhang et al. 2022). When computing the  $b$  for acoustic emission associated with rock fractures, the amplitude of acoustic emission is generally utilized to indicate the size of the event. By dividing the amplitude by 20, an equivalent seismic magnitude is obtained, which allows for a rough correspondence between the distributions of acoustic emission amplitudes and seismic magnitudes. Consequently, during indoor experimental acoustic emission studies, the formula for the  $b$  of acoustic emission is adjusted as proposed in (Sagasta et al. 2018)

$$\log_{10} N = a - bA_{\text{dB}}/20, \quad (7)$$

where  $A_{\text{dB}}$  represents the amplitude of the acoustic emission event.

To analyze the evolutionary pattern of  $b$  values of acoustic emission for partial anchorage and full-length anchorage joint surfaces, dynamic  $b$  values of acoustic emission during shear processes were calculated using Eq. (7) based on amplitude data, as shown in Fig. 16. From Fig. 16, it can be observed that the variations in acoustic emission amplitude and  $b$  values differ across different stages. Under the partial anchorage configuration: In Stage  $I_p$ , the distribution frequency of acoustic emission amplitude reaches the peak, and the  $b$  value rapidly decreases. This suggests that around the shear stress peak, acoustic emission signals are most active, and a relatively high proportion of large cracks are generated. In Stage  $II_p$ , although the distribution frequency of acoustic emission amplitude decreases, the  $b$  value remains at a low level. This indicates that acoustic emission signals gradually decrease during this stage, but the proportion of large cracks remains relatively high. In Stage  $III_p$ , the distribution frequency of amplitude is lower than in Stage  $II_E$ , but the  $b$  value starts to increase rapidly and then stabilizes. This suggests that the generation of acoustic emission signal further diminishes during this stage, primarily manifesting as small-scale microcracks. In Stage  $IV_p$ , the distribution frequency of acoustic emission amplitude further decreases, and the  $b$  value experiences a slight decline, but still remains higher than in Stage  $I_E$ . This is due to the fact that after the partial anchorage bolt breaks, it remains protruding from the joint surface, and interaction between the fractured bolt and the joint surface continues, generating significant acoustic emission signals. Consequently, although the quantity of acoustic emission signals decreases further during this stage, the proportion of large cracks being generated relatively increases. Under the full-length anchorage configuration: In Stage  $I_F$ , similar to the partial anchorage configuration, the distribution frequency of acoustic emission amplitude reach the peak, and the  $b$  value rapidly decreases. This indicates high acoustic emission activity around the shear stress peak and a higher proportion of large cracks being generated. In Stage  $II_F$ , as shear displacement increases, the distribution frequency of acoustic emission amplitude decreases, and the  $b$  value remains at a low level while decreasing. This suggests that acoustic emission signals gradually decrease during this stage, but the proportion of large cracks remains relatively high. In Stage  $III_F$ , the distribution frequency of acoustic emission amplitude further decreases, and the overall trend of the  $b$  value is upward, while some  $b$  values show a downward trend. This phenomenon is related to the interaction between fractured bolts and joints after bolt failure. When the broken bolt is above the joint surface, it continues to interact with the joint surface, generating significant acoustic emission signals. However, when the broken bolt does not come

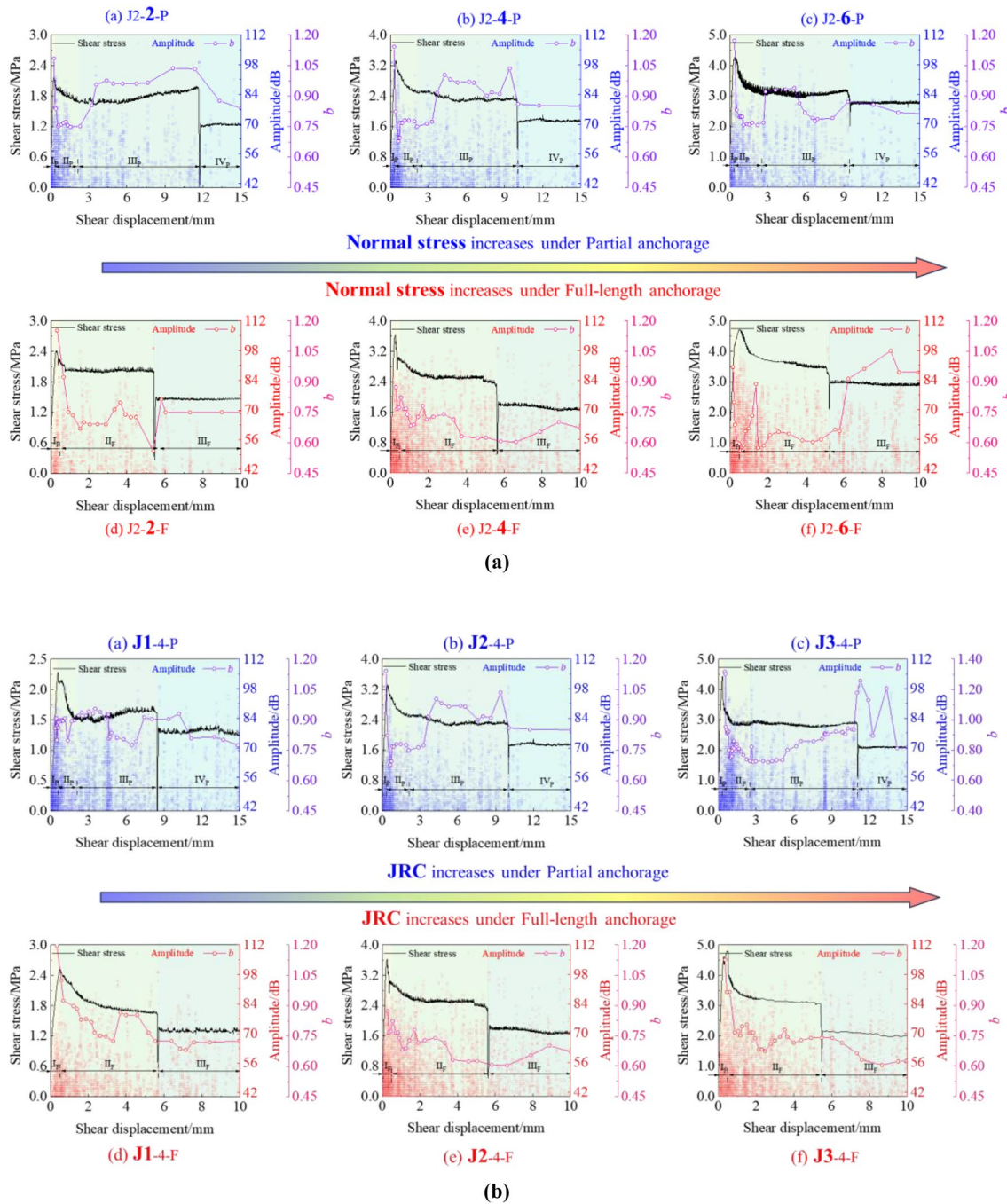


**Fig. 16** The amplitude and dynamic  $b$  values of acoustic emission of joint surfaces under different anchorage lengths: **a** the influence of normal stress; **b** the influence of joint roughness

into contact with the joint surface, the acoustic emission signals during this stage are smaller. Comparing the evolutionary patterns of  $b$  of acoustic emission under the partial anchorage and full-length anchorage configurations, it can be observed that before shear displacement reaches 3 mm, the variation trends of  $b$  value are approximately consistent for both anchorage lengths. As shear progresses, the  $b$  value rapidly decreases and then stabilizes. Subsequently, before

bolt failure, with increasing shear displacement, the  $b$  value under the partial anchorage configuration is higher than that under the full-length anchorage configuration. This reflects that, within this range, a higher proportion of large cracks are generated under the full-length anchorage configuration, indicating more intense interaction between the bolt and the surrounding rock in the full-length anchorage configurations.

From Fig. 16a, it can be observed that under the same Joint Roughness Coefficient (JRC) conditions, the  $b$  values of acoustic emission for both partial anchorage and full-length anchorage configurations decrease as the normal stress increases. Additionally, Fig. 16b indicates that under the same normal stress conditions, the  $b$  values of acoustic emission for both anchorage lengths generally decrease with an increase in JRC. This suggests that as the normal stress and JRC increase, the proportion of large cracks generated during the shear process of joint surface anchoring also increases.

By analyzing the evolution of acoustic emission characteristic parameters and  $b$  values, the differences in damage evolution characteristics between the partial anchorage and full-length anchorage configurations can be effectively revealed. This analysis contributes to a deeper understanding of the failure mechanisms of joint surfaces under different anchorage lengths and provides essential data support for identifying the precursory information of joint surface instability in a rational manner. Moreover, it has significant practical implications for enhancing rock engineering safety and protection, as well as disaster early warning systems.

## 6 Conclusion

This study conducted a series of rock joint shear tests under both full-length anchorage and partial anchorage configurations, revealing the shear mechanical characteristics of anchor joint and evolution pattern of acoustic emission features. Besides, the influences of anchorage lengths, normal stress, and joint surface roughness, shedding light on the shear damage mechanisms of rock joints under different anchorage lengths were elucidated. The following key conclusions were drawn:

- (1) The full-length anchorage demonstrated a quicker activation of the “pin effect” and higher peak shear stress compared to the partial anchorage. However, the fracture shear stress between the full-length anchorage and partial anchorage shows less variance, with a difference spanning 0.03 to 0.08 MPa.
- (2) Bolt deformation was about double in the partial anchorage compared to full-length anchorage. Under full-length anchorage, increased normal stress or Joint Roughness Coefficient (JRC) reduced bolt deformation, while in partial anchorage, increased normal stress decreased deformation, but higher JRC expanded it.
- (3) Analysis of the DDS curves reveals that the full-length anchorage reinforces joint shear strength more effectively than the partial anchorage before the full-length

anchorage bolt fails; but, after the full-length anchorage bolt failure, the situation reverses. This suggests that the full-length anchorage is suitability for projects requiring strict control of surrounding rock deformation. In contrast, partial anchorage is better for projects with lower deformation control needs.

- (4) Differences in internal joint damage under each anchorage length were evident in the variations of hit and energy patterns in acoustic emissions. The full-length method showed more intense interaction (higher hit rate) but less energy release upon bolt failure.
- (5) Higher normal stress or JRC led to a decrease in acoustic emission  $b$  values for both anchorage lengths, indicating more significant or faster growing cracks. The full-length method generally showed lower  $b$  values, suggesting greater damage within the bolted joints.

**Acknowledgements** This study is funded by the National Natural Science Foundation of China (No. 52104093) and the Shandong Provincial Natural Science Foundation (No. ZR2021QE069). These supports are gratefully acknowledged.

**Funding** National Natural Science Foundation of China, No. 52104093, Hengjie Luan, Shandong Provincial Natural Science Foundation, No. ZR2021QE069, Hengjie Luan

**Data Availability** The data generated in this study can be acquired from the corresponding author upon reasonable request.

## Declarations

**Conflicts of interest** The authors declare no conflict of interest.

## References

- Bahrani N, Hadjigeorgiou J (2017) Explicit reinforcement models for fully-grouted rebar rock bolts. *J Rock Mech Geotech Eng* 9(2):267–280
- Barton N, Choubey V (1977) The shear strength of rock joints in theory and practice. *Rock Mech Rock Eng* 10:1–54
- Chen Y, Li C (2015) Performance of fully encapsulated rebar bolts and D-Bolts under combined pull-and-shear loading. *Tunn Undergr Sp Tech* 45:99–106
- Chen N, Zhang X, Jiang Q, Feng X, Wei W, Yi B (2018) Shear behavior of rough rock joints reinforced by bolts. *Int J Geomech* 18(1):4017130
- Chen W, Zhao Z, Zhao Y (2018) Theoretical analysis on shear resistance of bolt under shear loading. *Chin J Undergr Sp Eng* 14(3):650–656
- Chen Y, Teng J, Sadiq RAB, Zhang K (2020) Experimental study of bolt-anchoring mechanism for bedded rock mass. *Int J Geomech* 20(4):04020019
- Cheng T, Wang LX, Xiao YM, He MC, Wang TZ, Peng ML, Li HR (2023) Correlational fractal characteristics and damage progression of granite with different grain sizes based on acoustic emission monitoring. *Eng Geol* 327:107358

- Cui G, Zhang Chuan Q, Chen J, Yang F, Zhou H, Lu J (2020) Effect of bolt inclination angle on shear behavior of bolted joints under CNL and CNS conditions. *J Cent South Univ* 27(3):937–950
- Fan H, Li L, Zong P, Liu H, Yang L, Wang J, Sun S (2023) Advanced stability analysis method for the tunnel face in jointed rock mass based on DFN-DEM. *Undergr Space* 13:136–149
- Feng C, Liu S, Fu M, Yao B, Jia H, He D (2024) Failure mechanism and strengthening countermeasures of end anchored cable free section under combined tension and shear. *Eng Fail Anal* 157:107949
- Ge XR, Liu JW (1988) Study on the shear resistance behaviour of bolted rock joints. *Chin J Geotech Eng* 10(1):8–19
- Grasselli G (2005) 3D Behaviour of bolted rock joints: experimental and numerical study. *Int J Rock Mech Min Sci* 42(1):13–24
- Grasselli G, Wirth J, Egger P (2002) Quantitative three-dimensional description of a rough surface and parameter evolution with shearing. *Int J Rock Mech Min Sci* 39(6):789–800
- Gutenberg B, Richter CF (1945) Frequency of earthquakes in California. *Nature* 156:371. <https://doi.org/10.1038/156371a0>
- He MC (2017) Technological progress promotes scientific coal production capacity to a higher level. *Sci News* 10:90
- He D, Yang W, Lin H, Cao R, Cheng Y (2019) Numerical analysis for direct shear test of bolted joint based on particle flow code. *J Eng Geol* 27(2):302–310 (**(in Chinese)**)
- He MC, Wang Q, Wu QY (2021) Innovation and future of mining rock mechanics. *J Rock Mech Geotech* 13(1):1–21
- Hu J, Pan H, Liu H, Li L, Fan H, Liu Q (2023) Response of acoustic emission and vibration monitoring data during rock block collapse in the tunnel: Small-and large-scale experiments study. *Tunn Undergr Sp Tech* 137:105121
- Jalalifar H, Aziz N (2010) Analytical behaviour of bolt-joint intersection under lateral loading conditions. *Rock Mech Rock Eng.* <https://doi.org/10.1007/s00603-009-0032-6>
- Jia Z, Xie H, Zhang R, Li C, Wang M, Gao M, Zhang Z, Zhang Z (2020) Acoustic emission characteristics and damage evolution of coal at different depths under triaxial compression. *Rock Mech Rock Eng.* <https://doi.org/10.1007/s00603-019-02042-w>
- Jiang YJ, Xiao J, Tanabashi Y, Mizokami T (2004) Development of an automated servo-controlled direct shear apparatus applying a constant normal stiffness condition. *Int J Rock Mech Min* 41(2):275–286
- Jiang YJ, Li XP, Liu JK, Luan HJ, Zhang SH, Wang CS, Wang D (2023) Study on shear behavior and failure characteristics of bolted anisotropic rock joints. *Materials* 16(6):2210
- Jiang YJ, Li XP, Wang CS, Luan HJ, Zhang SH, Wang G, Wang P (2023) Influence of normal stiffness and shear rate on the shear behaviors and acoustic emissions characteristics of artificial rock joints. *Appl Sci* 13(2):1189
- Jiang YJ, Zhang SH, Luan HJ, Chen LJ, Zhang GC, Wang CS (2023) Numerical investigation on the effect of cyclic loading on macro-meso shear characteristics of rock joints. *J Chin Coal Soc* 48(1):199–211
- Jiang YJ, Zhang SH, Luan HJ, Wang CS, Wang G, Han W (2022) Numerical modeling of the performance of bolted rough joint subjected to shear load. *Geomech Geophys Geo.* <https://doi.org/10.1007/s40948-022-00447-6>
- Jing HW, Yang SQ, Zhang ML, Xu GA, Chen KF (2014) An experimental study on anchorage strength and deformation behavior of large-scale jointed rock mass. *Tunn Undergr Sp Tech* 43:184–197
- Kang HP, Cui QJ, Hu B, Wu ZG (2014) Analysis on anchorage performances and affecting factors of resin bolts. *J China Coal Society* 39(1):1–10
- Li C (2017) Principles of rock bolting design. *J Rock Mech Geotech* 9(3):396–414
- Li SC, Wang HT, Wang Q (2016) Failure mechanism of bolting support and high-strength bolt-grouting technology for deep and soft surrounding rock with high stress. *J Cent South Univ* 23:440–448
- Li X, Yang G, Jan N, Mirzaghobanali A, Aziz N (2019) Numerical investigation of the shear behavior of a cable bolt in single shear test. *Tunn Undergr Sp Tech* 84:227–236
- Li W, Li X, Mei Y, Wang G, Yang W, Wang H (2022) A numerical simulation approach of energy-absorbing anchor bolts for rock engineering. *International J Rock Mech Min Sci* 158:105188
- Li S, Lin H, Feng J, Cao R, Hu H (2022) Mechanical properties and acoustic emission characteristics of anchored structure plane with different JRC under direct shear test. *Materials* 15(12):4169
- Li G, Wang J, Liu J, Chen J, Zhao H, Luan H, Dong Q, Zhang S (2022) Study on shear properties and failure characteristics of bolted joint of roadway surrounding rock. *J Shandong Univ Sci Technol* 41(4):47–55
- Li Y, Su G, Liu X, Wang L, Cao G, Pang G (2023) Laboratory study of the effects of grouted rebar bolts on shear failure of structural planes in deep hard rocks. *Int J Rock Mech Min Sci* 162:105308
- Lin H, Xiong Z, Liu T, Cao R, Cao P (2014) Numerical simulations of the effect of bolt inclination on the shear strength of rock joints. *Int J Rock Mech Min Sci* 66:49–56
- Liu A, Ju W (2012) Analysis of shear resisting action of full-length anchored bolt with pre-stress. *Coal Min Technol* 17(01):45–48
- Liu C, Li Y (2017) Analytical study of the mechanical behavior of fully grouted bolts in bedding rock slopes. *Rock Mech Rock Eng.* <https://doi.org/10.1007/s00603-017-1244-9>
- Liu C, Jiang Q, Xin J, Wu S, Liu J, Gong F (2022) Shearing Damage Evolution of Natural Rock Joints with Different Wall Strengths. *Rock Mech Rock Eng.* <https://doi.org/10.1007/S00603-021-02739-X>
- Liu C, Li Y (2018) Research progress in bolting mechanism and theories of fully grouted bolts in jointed rock masses. *Chin J Rock Mech Eng* 37(08):1856–1872
- Ma S, Zhao Z, Shang J (2019) An analytical model for shear behaviour of bolted rock joints. *Int J Rock Mech Min Sci* 121:104019
- Ma H, Song Y, Yang J, Zhen J, Shen F, Shao Z, Xia Z (2023) Experimental Investigation on Physical-Mechanical Behaviors and Macro-Micro-structural Responses of Lignite Subjected to Freeze-Thaw Cycles. *Nat Resour Res* 32(2):543–566
- Maiolino S (2015) Full scale lab testing for the determination of rock bolt contribution to reinforced joint shear strength. In *ISRM Congress (pp. ISRM-13CONGRESS)*. ISRM.
- Meng F, Zhou H, Li S, Zhang C, Wang Z, Kong L, Wang L (2016) Shear behaviour and acoustic emission characteristics of different joints under various stress levels. *Rock Mech Rock Eng.* <https://doi.org/10.1007/s00603-016-1034-9>
- Meng F, Wong LNY, Zhou H, Yu J, Chen J (2019) Shear Rate Effects on the Post-peak Shear Behaviour and Acoustic Emission Characteristics of Artificially Split Granite Joints. *Rock Mech Rock Eng.* <https://doi.org/10.1007/s00603-018-1722-8>
- Pellet F, Egger P (1996) Analytical model for the mechanical behaviour of bolted rock joints subjected to shearing. *Rock Mech Rock Eng* 29:73–97
- Sagasta F, Zitto M, Piotrkowski R, Amadeo BC, Elisabet S, Antolino G (2018) Acoustic emission energy b-value for local damage evaluation in reinforced concrete structures subjected to seismic loadings. *Mech Syst Signal Pr* 102:262–277
- Spang K, Egger P (1990) Action of fully-grouted bolts in jointed rock and factors of influence. *Rock Mech Rock Eng* 23(3):201–229. <https://doi.org/10.1007/BF01022954>
- Srivastava LP, Singh M (2015) Effect of fully grouted passive bolts on joint shear strength parameters in a blocky mass. *Rock Mech Rock Eng.* <https://doi.org/10.1007/s00603-014-0615-8>

- Teng JY, Zhang YN, Tang JX, Zhang C, Li CL (2017) Experimental study on shear behavior of jointed rock mass with anchorage mode. *Rock Soil Mech* 38(8):2279–2285
- Tse R, Cruden DM (1979) Estimating joint roughness coefficients. *Int J Rock Mech Min Sci Geomech Abstr* 16:303–307
- Wang G, Zhang Y, Jiang Y, Liu P, Guo Y, Liu J, Ma M, Wang K, Wang S (2018) Shear behaviour and acoustic emission characteristics of bolted rock joints with different roughnesses. *Rock Mech Rock Eng*. <https://doi.org/10.1007/s00603-018-1438-9>
- Wang J, Fu J, Song W, Zhang Y (2021) Mechanical properties, damage evolution, and constitutive model of rock-encased backfill under uniaxial compression. *Constr Build Mater* 285:122898
- Wang H, Liu X, Wang X, Zhou X, Xie H, Cai D, Gu P (2023) Stress-induced AE varying characteristics in distinct lithologies subjected to uniaxial compression. *Eng Fract Mech* 286:109266
- Wang C, Jiang Y, Wang G, Luan H, Zhang Y, Zhang S (2022) Experimental investigation on the shear behavior of the bolt-grout interface under CNL and CNS conditions considering realistic bolt profiles. *Geomech Geophys Geo*. <https://doi.org/10.1007/s40948-022-00416-z>
- Wang B, Jiang YJ, Zhang QY, Chen HB, Liu RC, Zhang YC (2024) Cyclic shear behavior of en-echelon joints under constant normal stiffness conditions. *J Rock Mech Geotech*. <https://doi.org/10.1016/j.jrmge.2023.12.002>
- Wu X, Jiang Y, Li B (2018) Influence of joint roughness on the shear behaviour of fully encapsulated rock bolt. *Rock Mech Rock Eng*. <https://doi.org/10.1007/s00603-017-1365-1>
- Wu X, Jiang Y, Gong B, Deng T, Guan Z (2018) Behaviour of rock joint reinforced by energy-absorbing rock bolt under cyclic shear loading condition. *Int J Rock Mech Min Sci* 110:88–96
- Wu SC, Chen L, Cheng ZQ (2019) Macro and meso research on the zonal disintegration phenomenon and the mechanism of deep brittle rock mass. *Eng Fract Mech* 211:254–268
- Xie H (2019) Research review of the state key research development program of China: Deep rock mechanics and mining theory. *J China Coal Society* 44(5):1283–1305 ((in Chinese))
- Yan S, Song Y, Bai J, Elmo D (2019) A study on the failure of resin end anchorage rock bolts subjected to tensile load. *Rock Mech Rock Eng* 52:1917–1930
- Yang N, Li WT, Xuan C, Zhang YH, Li DY, Li TC, Wang G (2017) Improvement of breakable anchor bolt element in flac3d and its application in deep coal roadway. *J Min Saf Eng* 34:251–258
- Yang RS, Li YL, Guo DM, Yao L, Yang TM, Li TT (2017) Failure mechanism and control technology of water-immersed roadway in high-stress and soft rock in a deep mine. *Int J Min Sci Technol* 27:245–252
- Yu G, Zhang Q, Li F, Cheng L, Guo X (2021) Physical model tests on the effect of anchoring on the splitting failure of deep large-scale underground rock cavern. *Geotech Geol Eng* 39:4545–4562
- Yu X, Song W, Tan Y, John K, Wang J (2022) Energy dissipation and 3d fracturing of Backfill-encased-rock under triaxial compression. *Constr Build Mater* 341:127877
- Zhang Q, Zhang X (2017) A numerical study on cracking processes in limestone by the b value analysis of acoustic emissions. *Comput Geotech* 92:1–10
- Zhang C, Cui G, Deng L, Zhou H, Lu J, Dai F (2020) Laboratory investigation on shear behaviors of bolt-grout interface subjected to constant normal stiffness. *Rock Mech Rock Eng*. <https://doi.org/10.1007/s00603-019-01983-6>
- Zhang YC, Jiang YJ, Daisuke A, Wang CS (2020) Experimental and numerical investigation on shear failure behavior of rock-like samples containing multiple non-persistent joints. *Rock Mech Rock Eng*. <https://doi.org/10.1007/s00603-020-02186-0>
- Zhang YC, Jiang YJ, Wang Z, Yin Q, Chen M (2022) Anchorage effect of bolt on en-echelon fractures: a comparison between energy-absorbing bolt and conventional rigid bolt. *Eng Fail Anal* 137:10625

**Publisher's Note** Springer Nature remains neutral with regard to jurisdictional claims in published maps and institutional affiliations.

Springer Nature or its licensor (e.g. a society or other partner) holds exclusive rights to this article under a publishing agreement with the author(s) or other rightsholder(s); author self-archiving of the accepted manuscript version of this article is solely governed by the terms of such publishing agreement and applicable law.